Research Square

Preprints are preliminary reports that have not undergone peer review.
They should not be considered conclusive, used to inform clinical practice,
or referenced by the media as validated information.

Simulation of winter wheat response to saline irrigation using AquaCrop in the Tadla Plain, Morocco: Implications for irrigation management

Khadija Manhou

khadija.manhou@uit.ac.ma

Laboratory of Natural Resources and Sustainable Development, Department of Biology, Faculty of Sciences, Ibn Tofail University, Kenitra 14000, Morocco

Rachid Moussadek

International Center for Agricultural Research in the Dry Areas (ICARDA), Rabat 10100, Morocco

Abdelmjid Zouahri

Research Unit on Environment and Conservation of Natural Resources, Regional Center of Rabat, National Institute of Agriculture Research (INRA), Avenue Ennasr, Rabat 10101, Morocco

Zoubida Belmahi

Research Unit on Environment and Conservation of Natural Resources, Regional Center of Rabat, National Institute of Agriculture Research (INRA), Avenue Ennasr, Rabat 10101, Morocco

Majda Oueld Lhaj

Laboratory of Process Engineering and Environment, Faculty of Science and Technology Mohammedia, University Hassan II of Casablanca, Mohammedia 28806, Morocco

Hatim Sanad

Laboratory of Process Engineering and Environment, Faculty of Science and Technology Mohammedia, Hassan II of Casablanca, Mohammedia 28806, Morocco

Hasna Yachou

Research Unit on Environment and Conservation of Natural Resources, Regional Center of Rabat, National Institute of Agricultural Research, AV. Ennasr, Rabat 10101, Morocco

Driss Hmouni

Laboratory of Natural Resources and Sustainable Development, Department of Biology, Faculty of Sciences, Ibn Tofail University, Kenitra 14000, Morocco

Houria Dakak

Research Unit on Environment and Conservation of Natural Resources, Regional Center of Rabat, National Institute of Agricultural Research, AV. Ennasr, Rabat 10101, Morocco

---

Research Article

Keywords: AquaCrop, saline irrigation, winter wheat, biomass, grain yield, soil salinity

Posted Date: April 29th, 2026

DOI: https://doi.org/10.21203/rs.3.rs-9534817/v2

License: This work is licensed under a Creative Commons Attribution 4.0 International License. Read Full License

Additional Declarations: The authors declare no competing interests.

Abstract

Saline irrigation is increasingly practiced in semi-arid regions to cope with freshwater scarcity; however, it strongly affects crop growth, water use, and soil salinity. This study aims to calibrate and validate the AquaCrop model to simulate key growth parameters of winter wheat (cv. Achtar) under saline irrigation conditions in the Tadla Plain, Morocco, focusing on canopy cover (CC), actual evapotranspiration (ETa), soil water content (SWC), biomass (B), and grain yield (GY). The model was first calibrated using observed data from the 2023 growing season and subsequently validated using data from the 2022 growing season. Overall, AquaCrop effectively reproduced crop growth during both calibration and validation phases. During calibration, canopy cover was accurately simulated, with average RMSE values below 1%, while biomass and grain yield were also well reproduced, with low RMSE values (0.25 t ha^{-1} for B and 0.10 t ha^{-1} for GY), confirming the robustness of the calibrated parameters. The model also performed well in simulating ETa and SWC, capturing the seasonal dynamics of crop water use and soil moisture. During validation, ETa was satisfactorily reproduced, with an RMSE of approximately 0.80 mm day^{-1}, while SWC showed good agreement with observations, with NRMSE values ranging from 7.9 to 10.5%. Grain yield and biomass were reliably predicted, with NRMSE values below 4%. These results demonstrate that AquaCrop is a reliable tool for simulating winter wheat under saline irrigation and for assessing crop response under salt-affected conditions, providing an integrated evaluation of crop performance, water use, and soil salinity dynamics to support improved irrigation management and water-use efficiency under semi-arid conditions.

1. Introduction

In arid and semi-arid regions, agriculture faces increasing challenges due to limited freshwater availability and progressive soil salinization, which are often exacerbated by high evaporation rates, prolonged droughts, and the allocation of high-quality water to urban and industrial sectors. Soil salinization, resulting from both natural processes and human activities such as insufficient irrigation, inadequate drainage, and overuse of fertilizers negatively impact soil structure, fertility, plant development, and crop productivity [1, 2]. The global population is expected to reach 9.7 billion by 2050, which will increase the challenge of ensuring sufficient, safe, and nutritious food for all [3]. Agriculture already accounts for approximately 70–75% of global freshwater withdrawals, highlighting the pressure on water resources to meet growing food demand [4]. However, the expansion of water use in agriculture is expected to be limited to around 10%, emphasizing the urgent need for efficient water management strategies directly applicable at farm level. The use of alternative water sources, including saline groundwater, drainage water, or treated wastewater, can help sustain crop growth, but also introduces challenges such as salt accumulation, increased sodicity, and degradation of soil physical properties, reducing root development, infiltration, and long-term fertility [4–7]. Such challenges highlight the need for site-specific irrigation strategies that maintain crop productivity while limiting soil degradation. Climatic variability, characterized by irregular rainfall, high evapotranspiration, and extreme weather events, further exacerbates water scarcity and soil salinization, threatening crop productivity and food security.

Winter wheat (*Triticum aestivum* L.) is a staple crop essential for global food security, providing over 20% of the calories consumed worldwide and serving as a major economic resource, particularly in Mediterranean and semi-arid regions [8–10]. Its grains, mainly used for bread, pastries, and other nutritionally and commercially valuable cereal products, are moderately sensitive to salinity, particularly during critical growth stages such as germination, tillering, stem elongation, and grain filling, which can significantly affect yield and quality under saline conditions [11]. Inadequate or saline irrigation can adversely affect wheat yield components, including spike density, grain filling rate, and thousand-grain weight, as well as grain quality through reductions in protein content and gluten strength [12–14]. These impacts can be mitigated by optimized irrigation practices that consider both water quality and quantity, as other environmental stresses such as drought and high temperatures further impact crop growth, water productivity, and yield stability [15–17]. In semi-arid and arid regions, where rainfall meets only a fraction of the crop's water requirements, irrigation is

critical to achieve high yield [18]. However, intensive use of groundwater has caused declining water tables, threatening the sustainability of production. Therefore, strategic use of marginal, saline, or brackish water becomes a practical solution to sustain wheat productivity while conserving high-quality freshwater, highlighting the vital importance of water availability and quality for winter wheat cultivation in water-limited areas [19].

To optimize winter wheat production under limited water availability and salinity stress, field experiments remain essential. They enable the evaluation of different management strategies and provide a better understanding of the interactions between soil, plants, and the atmosphere, as well as their effects on growth, yield, and stress tolerance [19–21]. Winter wheat, being moderately salt-tolerant, has a soil salinity threshold of approximately 6 dS m^{-1} and an irrigation water salinity threshold of around 4 dS m^{-1}, beyond which yield can be significantly reduced. This moderate tolerance necessitates the implementation of management practices that specifically limit salt accumulation in the root zone to sustain productivity [23–26]. Deficit irrigation using slightly saline water, adjusted to the crop's critical water requirements, appears more effective than excessive irrigation, which can reduce water use efficiency and cause nutrient losses [27–29]. Rainfall, which influences both salt leaching and crop performance, should also be considered when planning irrigation [30].

Among the available tools for simulating crop growth and water use, the FAO-developed AquaCrop model is particularly effective for predicting winter wheat yield, biomass, canopy cover, and water productivity under water-limited and saline conditions [31]. Crop growth simulations depend on complex interactions among climate, soil, plant, and management factors, and many models require extensive input data, limiting their practical application. In contrast, AquaCrop adopts a water-driven approach and integrates soil water and solute transport processes using a relatively small set of parameters, allowing efficient simulation of salinity dynamics and crop response to salt stress [32, 33]. Compared with more complex models such as SWAP, HYDRUS, and SALTMED, AquaCrop provides a balance between simplicity and accuracy, facilitating calibration and validation for practical use [34–37]. Although AquaCrop has been successfully applied across various crops and environments [38, 39], studies combining field-based calibration, independent validation without parameter adjustment, and multi-year simulations under contrasting climatic conditions remain limited [38–39]. Addressing this gap is essential to improve model applicability under variable farming conditions. Therefore, this study aims to evaluate the performance of AquaCrop under combined salinity and semi-arid conditions using detailed field measurements and independent validation datasets. The integration of field observations with multi-year simulations provides a robust framework for assessing model reliability and supporting improved irrigation management.

Building upon this approach, the study integrates field-based calibration and validation with multi-year AquaCrop simulations to improve saline irrigation management under water-limited and salt-affected conditions. Particular emphasis is placed on ensuring the practical applicability of the modeling approach by incorporating realistic irrigation practices and salinity levels representative of field conditions. This framework enables a more accurate assessment of crop response under combined water and salinity stresses. Therefore, the specific objectives of this study were to: (i) calibrate the AquaCrop model under controlled saline irrigation conditions using field data covering a wide and realistic gradient of irrigation water salinity levels; (ii) validate the model using field observations to assess its predictive performance under varying salin-ity and water stress conditions; (iii) analyze the coupled interactions between crop growth, water use, and soil salinity dynamics by simultaneously evaluating plant and soil responses; (iv) apply the validated model to perform multi-year simulations under contrasting climatic conditions in order to assess model robustness under variable environmental conditions; and (v) identify salinity tolerance thresholds of the studied cultivar and develop practical, field-applicable irrigation strategies aimed at improving water-use efficiency while minimizing soil salinity risks.

2. Materials and methods

2.1. Field site description and experimental design

The Tadla Plain is a major WNW–ESE–oriented synclinal depression located in central Morocco, covering nearly 3600 km² between 32°28'49"–32°31'10" N and 6°42'21"–6°16'03" W (Fig. 1) [36–37] The basin is bordered to the north by the gently rising Phosphate Plateau and to the south by the Jurassic formations of the High Atlas Mountains. Toward the east, the plain narrows along the Oum Er-Rbia River as it approaches the rugged Zaian uplands, while its western extent merges gradually with the Bahira region; the lower reach of the El Abid River is commonly considered the hydrogeological boundary. It stretches approximately 125 km in length and up to 50 km in width, with elevations ranging from 350 to 500 m. The lowest point (315 m) is located at the Sidi Driss hydrological station along the Oum Er-Rbia [38] .

The Beni Amir irrigated perimeter has undergone substantial agricultural intensification since 1954, supported by fertile soils and reliable surface-water resources, making it one of the most productive sectors of the Tadla irrigation scheme [46]. The region experiences a semi-arid Mediterranean climate with marked seasonal contrasts. Rainfall is concentrated in winter and early spring, while a prolonged dry period typically spans from late May to mid-autumn. Long-term climatic observations indicate an average annual precipitation of about 393 mm [40], with March and April registering the highest monthly totals. Summers are extremely hot, with peak temperatures approaching 38°C, whereas winter nighttime temperatures may fall close to freezing. Atmospheric evaporative demand remains high throughout most of the year, reaching a maximum in July and August and declining substantially during winter. Reference evapotranspiration exceeds 1 000 mm per year, reflecting the strong climatic water deficit characteristic of the area. The field experiment was conducted on an experimental area of 33 m × 35 m, arranged according to a Randomized Complete Block Design (RCBD) with four replicates to account for spatial variability within the field. The soil of the experimental site was preliminarily surveyed to ensure relative homogeneity in texture and topography prior to plot establishment. Five irrigation water salinity treatments were evaluated: I0 (1.5 dS m^{-1}), I2 (3 dS m^{-1}), I3 (5 dS m^{-1}), I4 (7 dS m^{-1}), and I5 (9 dS m^{-1}). These treatments were randomly assigned within each block to avoid positional bias and ensure unbiased comparisons among salinity levels. Each experimental plot measured 5 m in length, and plots were separated by 3 m-wide buffer alleys to minimize lateral movement of salts and water between adjacent treatments and to facilitate field operations. Buffer zones were carefully maintained throughout the experiment to prevent cross-contamination among salinity treatments. Winter wheat was sown uniformly across all plots using identical row spacing and seeding density to ensure consistent crop establishment and growth conditions. All agronomic practices, including fertilization, weed control, and pest management, were applied uniformly across treatments following local agricultural practices, so that irrigation water salinity remained the only experimental factor [41].

2.2. Data Collection

2.2.1. Climatic Data

Meteorological measurements, including maximum and minimum air temperatures (Tmax and Tmin), mean temperature, wind speed (measured at 2 m height), relative humidity, solar radiation, and precipitation, were obtained from the CRAT meteorological station located in the Beni Amir irrigated area, approximately 9 km east of Fquih Ben Salah within the Tadla irrigated perimeter, Morocco, at 32°28'08" N, 06°41'24" W and 434 m asl, and operated by the Regional Office for Agricultural Development of Tadla (ORMVAT). These data were used to calculate reference evapotranspiration (ET_0) using the FAO Penman–Monteith equation [42].

Figure 2 presents the time series of ET_0, air temperature, and rainfall for the calibration (2023) and validation (2022) seasons. Daily ET_0 values ranged from approximately 2.1 to 8.1 mm day^{-1} during the calibration season and from 2.0 to

7.4 mm day^{-1} during the validation season, indicating a higher atmospheric evaporative demand in 2023. Thermal conditions differed between the two seasons. The calibration season recorded maximum air temperatures up to 47.8°C and minimum temperatures between 3.9 and 17.6°C, whereas the validation season exhibited slightly lower maximum temperatures (up to 46.3°C) and minimum temperatures ranging from 1.6 to 17.7°C. These differences suggest greater thermal stress during the calibration season, particu-larly during the mid- to late-growth stages, which may affect crop development and evapotranspiration dynamics.

Rainfall was low and irregular in both seasons but differed in distribution. The 2023 season received less than 200 mm with sparse events, whereas 2022 recorded higher rainfall exceeding 200 mm, with more frequent early-season precipitation, likely improving soil moisture availability and crop water uptake. In addition, long-term climatic data used for scenario analysis were obtained from the NASA POWER database [43], which provides open-access satellite-derived climatic data widely used in scientific research.

2.2.2. Soil Data

The soil profile used in AquaCrop was parameterized based on detailed laboratory analyses of soil samples collected prior to sowing. The soil was characterized down to a depth of 90 cm and subdivided into three layers (0–30, 30–60, and 60–90 cm). For each layer, particle-size distribution, pH, electrical conductivity (ECe), organic matter content, calcium carbonate, mineral nitrogen (NH_4^+ and NO_3^-), cation exchange capacity (CEC), bulk density, and hydraulic properties were determined. Soil samples were air-dried at room temperature to reach a stable moisture state, gently disaggregated, and sieved to < 2 mm. A subsample of this fraction was then further reduced to < 0.2 mm for chemical analyses. Particle-size distribution was determined using the sedimentation method after chemical dispersion, allowing the quantification of sand, silt, and clay fractions [51]. Soil pH was measured potentiometrically using a glass-electrode pH meter [52], while soil electrical conductivity was determined on the saturated paste extract using a calibrated conductivity meter [53]. Organic matter content was quantified following the Walkley–Black wet oxidation method [54], total nitrogen was determined using the Kjeldahl procedure [55], and CEC was measured by ammonium acetate extraction (1 N NH_4OAc) [56]. These measurements were used to derive the hydraulic parameters required by AquaCrop, including saturated water content (θsat), field capacity (FC), permanent wilting point (PWP), and saturated hydraulic conductivity (Ksat), ensuring consistency between soil texture, bulk density, and water retention behavior.

In addition to the initial characterization, soil samples were collected at four key phenological stages of winter wheat (tillering, stem elongation, anthesis, and physiological maturity) to monitor temporal changes in soil moisture and salinity. These multi-stage observations were used to evaluate the seasonal evolution of soil ECe under saline irrigation and to verify AquaCrop-simulated soil water content across the soil profile. Initial soil water content at sowing was determined gravimetrically for each soil layer and converted to volumetric values for model initialization. According to USDA classification standards, the soil at the experimental site was identified as clay loam throughout the 0–90 cm profile. The complete set of physico-chemical and hydraulic parameters presented in Table 1 was subsequently used to construct the soil input file for model calibration and long-term simulation scenarios.

Table 1

Soil textural, chemical, and hydraulic properties of the experimental field used for model calibration and validation. FC: Field capacity; PWP: Permanent wilting point; Ksat: Saturated hydraulic conductivity. Soil texture classification follows the United States Department of Agriculture (USDA) system.

Soil layer depth (cm)	Particle Size Distribution (%)			Soil texture
	Sand (%)	Silt (%)	Clay (%)	
0–30	37.75	33.18	28.9	Clay Loam
30–60	37.9	33.82	28.1	Clay Loam
60–90	36.3	31.41	29.4	Clay Loam

Chemical parameters								
	pH	ECe (dS m^{-1})	OM (%)	Total $CaCO_3$ (%)	NH_4^+	NO_3^-	Total mineral N	CEC (cmolc kg^{-1})
0–30	8.36	0.21	1.62	15.85	15.37	34.65	50.02	45.3
30–60	8.45	0.22	1.33	9.85	13.65	28.00	41.65	42.2
60–90	8.50	0.18	0.86	13.8	10.10	18.90	29.00	41.4

Physical and hydraulic parameters					
	Bulk Density (g cm^{-3})	Ksat (mm day^{-1})	Saturation (cm^3 cm^{-3})	FC (cm^3 cm^{-3})	PWP (cm^3 cm^{-3})
0–30	1.40	125	0.50	0.39	0.23
30–60	1.46	500	0.50	0.30	0.20
60–90	1.52	500	0.50	0.30	0.21

Soil texture classification follows the United States Department of Agriculture (USDA) system [44].

2.2.3. Crop Management

Winter wheat (cv. Achtar) was sown using a mechanical seed drill at a density of 300 seeds m^{-2} to ensure uniform crop establishment across all experimental plots. The experiment was conducted using microplots arranged in a randomized complete block design (RCBD) with four replications, allowing controlled application of irrigation and salinity treatments. Immediately after sowing, all plots were well irrigated to promote seed emergence and early seedling growth. The study was conducted over two growing seasons, with 2023 used for calibration and 2022 for validation. The cultivar was selected for its adaptability to irrigated systems, moderate tillering capacity, and semi-early to semi-late maturity cycle, making it suitable for the agroclimatic conditions of the study area (Table 2). Fertilization was applied uniformly across all treatments to avoid nutrient-induced variability, with a basal application of 200 kg ha^{-1} of triple superphosphate and 100 kg ha^{-1} of potassium sulfate at sowing, and a total nitrogen input of 150 kg ha^{-1} split into three applications (60, 30, and 60 kg N ha^{-1} at sowing, till-ering, and stem elongation, respectively). Crop protection practices were uniformly applied across seasons. The crop reached physiological maturity and was harvested in mid- to late June in both 2022 and 2023. All agronomic practices were kept consistent between seasons to ensure that differences in crop performance were primarily attributable to irrigation water salinity (Table 3).

Table 2
Agronomic and technological characteristics of the wheat variety Achtar. GW: Grain Weight; TW: Test Weight; PC: Protein Content; ZI: Zeleny Index; MQ: Milling Quality.

Wheat variety	Adaptation zone	Average yield (t ha^{-1})	Potential Yield (t ha^{-1})	Plant height (cm)	Tillering capacity	Maturity cycle	Lodging resistance	Technological traits
Achtar	Recommended for fertile soils and irrigated conditions	4.5	– 11.8 (irrigated), -11.2 (rainfed)	75–115	Medium	Semi-early to semi-late	Good	GW : 39.18 mg TW : 81 kg hl^{-1} PC : 13.4% ZI : 33 ml MQ : Good

Table 3
Summary of crop management practices, fertilization schedule, and phytosanitary treatments for winter wheat during the validation (2022) and calibration (2023) growing seasons.

Parameter	Validation	Calibration	Notes
Cultivar	Achtar	Achtar	Same cultivar both years
Growing season	Winter	Winter	—
Sowing date	24 Nov 2021	24 Nov 2022	—
Seeding rate	300 seeds m^{-2}	300 seeds m^{-2}	Uniform across plots
Basal P fertilization	200 kg ha^{-1} TSP	Same	At sowing
Basal K fertilization	100 kg ha^{-1} K_2SO_4 (45% K_2O)	Same	At sowing
Total N fertilization	150 kg ha^{-1}	150 kg ha^{-1}	Split into 3 applications
-N at sowing	40% as ammonium sulfate	Same	60 kg N ha^{-1}
-N at tillering	20% as ammonium nitrate	Same	30 kg N ha^{-1}
-N at stem elongation	40% as ammonium nitrate	Same	60 kg N ha^{-1}
Herbicide	Lintur (1 pack ha^{-1})	Same	Early vegetative stage (GS 14–15)
Nematicide	Furadan (10 kg ha^{-1})	Same	At sowing
Manual weeding	—	—	Stem elongation, GS 30–32)
Fungicide	Planète	Same	Flag leaf stage (GS 39–49)
Harvest date	Mid–late 2022	Mid–late June 2023	Physiological maturity

2.2.4. Irrigation Management

Irrigation was applied using a gravity-fed system supplied by a 3000 L tank to ensure uniform water distribution across all micro-plots. Each 15 m^2 plot received 1500 L per irrigation event, corresponding to an application depth of 100 mm (1000 m^3 ha^{-1}). Irrigation volume and delivery method were kept identical across treatments so that irrigation-water salinity remained the only experimental factor. Freshwater used for irrigation was groundwater abstracted from the Béni

Amir irrigated perimeter and served as the control treatment (1.5 dS m^{-1}). Five irrigation-water salinity levels (1.5, 3, 5, 7, and 9 dS m^{-1}) were selected to reflect the high spatial and temporal variability of irrigation water salinity in the Béni Amir area, where electrical conductivity ranges from 1.83 to 9 dS m^{-1}, with the 2–4 dS m^{-1} class being the most prevalent. This range therefore encompasses both commonly used irrigation waters and higher salinity conditions that may occur locally due to groundwater abstraction, water mixing, and water scarcity periods. Saline irrigation waters were prepared by adding controlled amounts of sodium chloride (NaCl) to the same groundwater source until the target electrical conductivity levels (3, 5, 7, and 9 dS m^{-1}) were reached. This method ensured stable, reproducible, and well-controlled salinity levels throughout the experiment. Electrical conductivity was measured before each irrigation event using a calibrated conductivity meter to maintain consistency among treatments. Irrigation during the 2022 and 2023 growing seasons was applied on four fixed dates (5 December, 28 January, 3 March, and 16 April), corresponding to key phenological stages of winter wheat and aligned with regional agronomic practices. Applying irrigation on identical dates across all treatments ensured comparable water supply conditions and isolated the effects of salinity from irrigation timing.The chemical characteristics of the irrigation water used in each treatment are summarized in Table 4 and were directly incorporated into the AquaCrop model to simulate osmotic stress and soil salinity dynamics [58].

Table 4
Chemical quality parameters of the irrigation water used in the experiment and WHO (2017) standards.

Parameters	Value	WHO (2017) Standards
pH	7.65	6.5–8.5
EC	1.20	1 dS m^{-1}
Ca^{2+}	3.03	75 mg/L
Mg^{2+}	2.34	50 mg/L
Na^{+}	16.97	200 mg/L
K^{+}	0.12	10 mg/L
Cl^{-}	16.15	250 mg/L
SO_4^{2-}	1.89	250 mg/L
HCO_3^{-}	3.81	120 mg/L
NO_3^{-}	5.00	50 mg/L

2.3. Description of the AquaCrop Model

The AquaCrop model, developed by the FAO [38, 39, 59], is a water-driven crop model used to simulate crop growth, biomass production, and yield under different environmental and management conditions. In this study, simulations were performed using AquaCrop version 7.1, released in August 2023. The model is based on the relationship between crop transpiration and biomass accumulation through a normalized water productivity parameter (WP), while grain yield is estimated using the harvest index (HI). Crop development is described using canopy cover (CC), which evolves from emergence to a maximum value and declines during senescence. The canopy cover curve, defined by the initial canopy cover (CC_0), canopy growth coefficient (CGC), maximum canopy cover (CCx), and canopy decline coefficient (CDC), is used to partition reference evapotranspiration into soil evaporation and crop transpiration.

To calculate transpiration, the model employs the equation:

$$Tr = K_S \times (K_{cTr,x} \times CC^*) \times ET_0 \quad (1)$$

Where Tr represents crop transpiration, $K_{cTr,x}$ denotes the maximum crop transpiration coefficient, CC* signifies the canopy cover (%), Ks denotes the stress coefficient, and ET_0 represents reference evapotranspiration.

The final above-ground dry biomass is estimated using the following equation:

$$B = WP^* \times \sum T_r \quad (2)$$

Where B is the final above-ground dry biomass (t ha^{-1}), WP* is the normalized water productivity (g m^{-2}), and $\sum T_r$ is the cumulative actual crop transpiration over the growing season (mm).

AquaCrop calculates dry grain yield using the following equation:

$$GY = B \times HI \quad (3)$$

Where B represents the final above-ground dry biomass (t ha^{-1}) and HI denotes the harvest index.

Figure 3. Calculation scheme of the AquaCrop model, showing the four sequential steps (A–D) and the associated processes (dotted arrows) affected by water stress (1–5) and temperature stress (6–7). CC is the green canopy cover; Zr is the rooting depth; CGC is the canopy growth coefficient; CDC is the canopy decline coefficient; GDD is the growing degree days; ET0 is the reference evapotranspiration; WP is the normalized biomass water productivity; and HI is the harvest index. Water stress: (1) slows canopy expansion, (2) accelerates canopy senescence, (3) decreases root deepening (only under severe stress), (4) reduces stomatal conductance and transpiration, and (5) affects the harvest index. Cold temperature stress (6) reduces crop transpiration, while extreme temperature stress (7) inhibits pollination and reduces HI [60].

2.4. Model calibration and validation

Calibration and validation are essential steps in model evaluation, as they reduce uncertainties and ensure that the model adequately represents the behavior of the system [61]. Model calibration involves identifying a set of parameters that best describe the system by comparing simulated outputs with observed data. Subsequently, model validation assesses the predictive capability of the model by evaluating its performance against independent observations [62]. In this study, the AquaCrop model was calibrated to simulate the growth, biomass production, and grain yield of winter wheat under the specific agro-climatic and irrigation conditions of the study area. At the initial stage of model parameterization, conservative parameters were retained at their default AquaCrop values, as they represent general crop characteristics and are not site-specific. Phenological development was defined based on field observations and expressed in growing degree days (GDD), which provide a robust representation of crop development under variable temperature conditions. In accordance with AquaCrop settings for wheat, a base temperature of 0°C and an upper temperature of 26°C were used. The timing of emergence, maximum canopy development, flowering, and the onset of senescence were derived directly from field observations, while the time to maturity was expressed in GDD and derived from the observed crop duration (Table 5).

The calibration procedure initially focused on canopy development, as canopy cover (CC) directly controls transpiration and biomass accumulation. Parameters governing canopy growth, including the initial canopy cover (CC_o), maximum canopy cover (CCx), canopy growth coefficient (CGC), and canopy decline coefficient (CDC), were adjusted to ensure good agreement between simulated and observed canopy cover dynamics. Subsequently, crop parameters influencing transpiration and biomass production were calibrated. The maximum crop transpiration coefficient ($K_{cTr,x}$), normalized crop water productivity (WP*), and reference harvest index (HI_o) were fine-tuned using an iterative trial-and-error approach to minimize discrepancies between simulated and observed biomass (B) and grain yield (GY), as recommended in AquaCrop applications [39]. The maximum effective rooting depth (Zr) was also calibrated to improve the simulation of soil water content (SWC) and actual evapotranspiration (ETa).

Soil water balance parameters, including curve number (CN) and readily evaporable water (REW), were maintained at their default values, as they are considered conservative parameters. Similarly, soil water depletion thresholds (Pexp, Psto, and Psen) and salinity response parameters were not modified. In contrast, salinity stress thresholds were adjusted to 5 and 18 dS m^{-1} to reflect local soil and irrigation conditions. Initial soil water content (SWC) was determined from field measurements prior to sowing and used as an input for model simulations, while temporal SWC measurements were used for calibration and validation.

Table 5
AquaCrop model parameters used for the calibration and validation of winter wheat (cv. Achtar).

Parameters	Values	Units	Determination way
Canopy cover parameters			
Initial canopy cover (CC_o)	5.25	%	Estimated
Maximum canopy cover (CCx)	96	%	Calibrated
Canopy growth coefficient (CGC)	0.52	% day^{-1}	Calibrated
Canopy decline coefficient (CDC)	0.39	% °C day^{-1}	Calibrated
Crop parameters			
Maximum coefficient for transpiration at CCx ($K_{cTr,x}$)	1.08	–	Calibrated
Normalized crop water productivity (WP*)	16.8	g m^{-2}	Calibrated
Reference harvest index (HI_o)	44	%	Calibrated
Maximum effective rooting depth (Zr)	1.10	m	Calibrated
Minimum effective rooting depth (Zmin)	0.30	m	Model default
Depletion of soil water thresholds			
Leaf expansion, upper threshold ($P_{exp,upper}$)	0.20	–	Model default
Leaf expansion, lower threshold ($P_{exp,lower}$)	0.65	–	Model default
Stomatal closure, upper threshold ($P_{sto,upper}$)	0.65	–	Model default
Upper threshold for canopy senescence ($P_{sen,upper}$)	0.70	–	Model default
Soil water balance parameters			
Curve number (CN)	72	–	Model default
Readily evaporable water (REW)	11	mm	Model default
Phenological parameters			
Time to emergence	150	°C d	Observed
Time to maximum canopy	1197	°C d	Observed
Time to maximum rooting depth	864	°C d	Calibrated
Time to start of senescence	1700	°C d	Observed
Time to maturity	2800	°C d	Derived from field observations
Time to flowering	1250	°C d	Observed
Duration of flowering	200	°C d	Observed
Length of HI build-up	1100	°C d	Calibrated
Salinity stress parameters			
Lower threshold for salinity stress	5	dS m^{-1}	Calibrated

Parameters	Values	Units	Determination way
Canopy cover parameters			
Upper threshold for salinity stress	18	dS m^{-1}	Calibrated
Canopy response to salinity	25	–	Model default
Stomatal closure response to salinity	115	–	Model default

2.5. Model evaluation

This study employed several statistical metrics to evaluate the performance of the AquaCrop model, including percent error (Pe, Eq. 4), root mean square error (RMSE, Eq. 5), normalized root mean square error (NRMSE, Eq. 6), the coefficient of determination (R2, Eq. 7) [63], and the index of agreement (d, Eq. 8). These indicators were used to assess the agreement between observed (Oi) and simulated (Pi) values of canopy cover (CC), soil water content (SWC), actual evapotranspiration (ETa), grain yield (GY) and biomass (B).

$$Pe = \left(\frac{Pi-Oi}{Oi}\right) \times 100 \quad (4)$$

$$RMSE = \sqrt{\frac{1}{n}\sum_{i=1}^{n}(Oi\text{-}Pi)^2} \quad (5)$$

$$NRMSE = \frac{RMSE}{\bar{O}} \times 100 \quad (6)$$

$$R^2 = \left[\frac{\sum_{i=1}^{n}(Oi\text{-}O^{-})(Pi\text{-}P^{-})}{\sqrt{\sum_{i=1}^{n}(Oi - \bar{O})^2} \times \sqrt{\sum_{i=1}^{n}(Pi - P)^2}}\right]^2 \quad (7)$$

$$d = 1 - \frac{\sum_{i=1}^{n}(Pi - Oi)^2}{\sum_{i=1}^{n}(Pi - Oi) + |Oi - P^{-}|)^2} \quad (8)$$

where Pi and Oi denote the simulated and observed values, respectively; P^{-} and O^{-} represent their corresponding means; and n is the total number of observations. These statistical indicators were used to quantify how well the simulated outputs matched the measured data during the calibration process. The evaluation metrics consisted of the coefficient of determination (R^2), which measures the quality of fit between observed and simulated datasets; the root mean squared error (RMSE), which expresses the average magnitude of the deviation between simulated and observed values; and the normalized root mean squared error (NRMSE, %), calculated as the ratio of RMSE to the mean of the observed dataset. In addition, the index of agreement (d) was used to assess the overall degree of agreement between simulated and observed values, with values approaching 1 indicating better model performance. Additionally, the relative error (Pe) was employed to identify whether the model systematically underestimates or overestimates the

observations. According to the NRMSE classification, model performance is considered excellent (< 10%), good (10–20%), fair (20–30%), or poor (> 30%)[64]. More detailed descriptions of these statistical metrics are provided in [65] and [66]. Figure 4 illustrates the schematic representation of the AquaCrop model input structure and workflow.

2.5. Irrigation Salinity Management Scenarios

After model calibration and validation, AquaCrop was used to analyze winter wheat performance and soil salinity dynamics under a range of irrigation and salinity conditions combined with contrasting climatic periods (1996–2007 and 2018–2023). To account for inter-annual rainfall variability, each simulation year was classified as dry (P < 200 mm), normal (200 ≤ P ≤ 260 mm), or wet (P > 260 mm), based on long-term rainfall variability in the study area. Irrigation scheduling was based on regional agronomic recommendations and consistent with the management applied during the 2023 field experiment (calibration dataset), ensuring coherence between observed and simulated conditions. Five irrigation scenarios (Sc1–Sc5) were defined to represent increasing irrigation intensity across wheat phenological stages, with each irrigation event supplying 100 mm of water. Specifically, Sc1 corresponds to a highly deficit irrigation strategy with a single irrigation applied at the jointing stage, while Sc5 represents full irrigation with five events applied before winter, at jointing, booting, flowering, and grain filling stages. Intermediate scenarios (Sc2–Sc4) represent progressively increasing irrigation inputs. For each irrigation scenario, seven irrigation-water salinity levels were considered, defined as I0 (1.5 dS m^{-1}), I1 (3 dS m^{-1}), I2 (5 dS m^{-1}), I3 (7 dS m^{-1}), I4 (9 dS m^{-1}), I5 (10 dS m^{-1}), and I6 (12 dS m^{-1}). These levels reflect the range of water quality sources commonly used in the Tadla region, including canal water, groundwater, and mixed or drainage water. This scenario-based approach was designed to systematically explore a wide range of crop responses under combined water and salinity stresses. By varying irrigation intensity and salinity levels across different climatic conditions, the simulations enabled the identification of trade-offs between crop productivity (grain yield and biomass) and soil salinity (ECe). Model outputs, including simulated grain yield (GY), biomass (B), and soil electrical conductivity (ECe), were analyzed to assess the combined and interactive effects of irrigation management, salinity, and climate variability.

3. Results

3.1. Calibration of AquaCrop Model

3.1.1. Simulation of canopy Cover

The calibration of canopy cover (CC) was used to assess the performance of the AquaCrop model under saline irrigation conditions (I0–I4). The model showed close agreement between simulated and observed values across all salinity treatments. It reproduced CC dynamics throughout the growing cycle, from emergence to maximum cover and subsequent decline. Model performance was high, with coefficients of determination (R^2 = 0.99) and low error metrics (RMSE = 0.75–0.89%; NRMSE = 1.94–2.88%). Prediction error (Pe) ranged from − 16.70 to − 0.10%, indicating a slight underestimation, more pronounced under higher salinity levels (I3 and I4). Overall, the model adequately captured canopy cover dynamics under varying salinity conditions (Fig. 5).

3.1.2. Simulation of grain yield and biomass

Table 6 presents the simulated and observed grain yield (GY) and above-ground biomass (B) under different salinity treatments (I0–I4), further evaluating model performance under saline conditions. Both GY and B decreased with increasing irrigation-water salinity. Grain yield declined from 4.31 t ha^{-1} (I0) to 3.80 t ha^{-1} (I3), and further to 2.60 t ha^{-1} under I4. Similarly, biomass decreased from 14.53 t ha^{-1} (I0) to 12.90 t ha^{-1} (I3), followed by a marked reduction to 8.80 t ha^{-1} under I4. The AquaCrop model simulated GY and biomass with good accuracy. R^2 values reached 0.98 for GY and

0.85 for biomass, with RMSE values of 0.10 and 0.25 t ha⁻¹, respectively. NRMSE values remained below 3% for both variables. Overall, the model adequately captured yield and biomass responses across the salinity gradient

Table 6
Statistical evaluation of observed versus simulated grain yield (GY) and above-ground biomass (B) of winter wheat under different saline irrigation treatments (I0–I4) during the 2023 growing season is presented. The table includes the observed and simulated mean values, percent difference (Diff. %), root mean squared error (RMSE, t ha⁻¹), normalized RMSE (NRMSE, %), and the coefficient of determination (R^2), providing a quantitative assessment of the model's performance.

Treatment (dS m^{-1})	Observed	Simulated	Observed	Simulated
	GY (t ha^{-1})		B (t ha^{-1})	
I0	4.31	4.28	14.53	14.45
I1	4.12	4.05	13.95	13.80
I2	3.95	3.88	13.30	13.10
I3	3.80	3.75	12.90	12.70
I4	2.60	2.55	8.80	8.60

Parameter	Unit	Observed mean	Simulated mean	Diff. %	RMSE (t ha^{-1})	NRMSE (%)	R^2
GY	t ha^{-1}	3.76	3.70	1.60	0.10	2.70	0.98
B	t ha^{-1}	12.30	12.13	1.40	0.25	2.00	0.85

3.1.3. Simulation of soil water content

The simulated and observed soil water content (SWC) under different salinity treatments (I0–I4) is presented in Fig. 6. SWC dynamics followed similar patterns between simulated and observed values across all treatments. SWC increased during the growing period, reached a maximum, and then declined toward the end of the season. The AquaCrop model reproduced SWC dynamics with acceptable agreement, with R^2 values ranging from 0.85 to 0.91. RMSE values varied between 0.50 and 0.70%, while NRMSE values ranged from 8.0 to 10.0%. Prediction error (Pe) ranged from + 1.5% to + 7.2%, indicating a slight overestimation, particularly under higher salinity levels. Model performance slightly decreased with increasing salinity, as reflected by lower R^2 and higher error values.

3.1.4. Simulation of evapotranspiration

Actual evapotranspiration (ETa) decreased consistently with increasing irrigation-water salinity, from 3.50 mm day^{-1} under I0 to 2.48 mm day^{-1} under I4, corresponding to an overall reduction of 29.30%. Intermediate treatments followed a gradual decline, confirming a consistent response of ETa to the salinity gradient. The AquaCrop model reproduced this pattern with moderate performance, as indicated by coefficients of determination (R^2) ranging from 0.47 to 0.65. The highest agreement was observed under I1 (R^2 = 0.65), whereas lower values under higher salinity levels (I3–I4; R^2 = 0.47–0.50) reflect increased variability between simulated and observed ETa under stress conditions. Under I0, the model showed moderate agreement (R^2 = 0.52) (Fig. 7).

3.1.5. Validation of AquaCrop model results

3.1.5.1. Canopy cover validation results

The validation results of canopy cover (CC) (Fig. 8) indicate that the AquaCrop model maintained a strong agreement between simulated and observed values across all salinity treatments. The high correlation coefficients (R = 0.98–0.99) confirm a robust linear relationship, demonstrating that the model accurately reproduced the temporal evolution of canopy cover during the validation season. The index of agreement (d = 0.97–0.99) further highlights the high level of consistency between simulated and observed CC, indicating that AquaCrop reliably captured both the magnitude and timing of canopy development. Error statistics showed a moderate increase compared with the calibration phase, as expected during validation. The RMSE values ranged from 1.35 to 1.62%, while NRMSE values varied between 3.10 and 4.10%, reflecting an acceptable level of deviation under independent conditions. Percent bias (Pe) values were consistently negative (–12.5 to – 17.5%), indicating a tendency of the model to slightly underestimate canopy cover, particularly under higher salinity levels.

3.1.5.2. Soil water content validation results

The validation results for soil water content (SWC) indicate that the AquaCrop model was able to reasonably reproduce the temporal dynamics of soil moisture under different irrigation-water salinity treatments (I0–I4) (Fig. 9). Both observed and simulated SWC values exhibited similar seasonal trends, characterized by an increase following irrigation events and a gradual decline during periods without water input. Across treatments, the coefficients of determination ranged from R^2 = 0.82 to 0.90, demonstrating a satisfactory correspondence between simulated and measured SWC throughout the growing season. Error statistics further confirmed acceptable model performance, with RMSE values between 0.55 and 0.75% and NRMSE values ranging from 7.88 to 10.50%, indicating moderate deviations between observed and simulated values under validation conditions. Percent error (Pe) values were consistently positive (+ 3.20 to + 4.80%), suggesting a slight overestimation of soil water content by the model across most salinity treatments. This tendency became more apparent under higher salinity levels (I0 and I4), where reduced crop water uptake and increased soil moisture retention may influence the accuracy of simulated SWC patterns.

3.1.5.3. Validation of grain yield and biomass

The validation results for grain yield (GY) and above-ground biomass (B) are presented in Table 7. Both observed and simulated values showed a decreasing trend with increasing irrigation-water salinity (I0–I4). Grain yield declined from 4.36 t ha^{-1} (I0) to 3.90 t ha^{-1} (I3), and further to 3.10 t ha^{-1} under I4, corresponding to a reduction of approximately 29% relative to the control. A similar pattern was observed for biomass, which decreased from 14.80 t ha^{-1} (I0) to 13.30 t ha^{-1} (I3), followed by a marked decline to 10.40 t ha^{-1} under I4. Model performance remained satisfactory, with NRMSE values below 4% and R^2 values above 0.90 for GY, and NRMSE below 3% and R^2 above 0.80 for biomass. Overall, the model adequately captured yield and biomass responses under validation conditions.

Table 7
Statistical evaluation of observed versus simulated grain yield (GY) and above-ground biomass (B) of winter wheat under different saline irrigation treatments (I0–I4) during the 2022 growing season. The table presents the observed and simulated mean values, percentage difference (%), root mean square error (RMSE, t ha⁻¹), normalized RMSE (NRMSE, %), and the coefficient of determination (R^2), providing a quantitative assessment of model validation performance.

Treatment (dS m^{-1})	Observed	Simulated	Observed	Simulated
	GY (t ha^{-1})		B (t ha^{-1})	
I0	4.36	4.30	14.80	14.55
I1	4.22	4.15	14.30	14.00
I2	4.05	3.98	13.80	13.55
I3	3.90	3.82	13.30	13.05
I4	3.10	2.95	10.40	10.10

Parameter	Unit	Observed mean	Simulated mean	Diff. %	RMSE (t ha^{-1})	NRMSE (%)	R^2
GY	t ha^{-1}	3.93	3.84	2.30	0.15	3.80	0.92
B	t ha^{-1}	13.32	13.05	2.00	0.32	2.40	0.84

3.1.5.4. Evapotranspiration Validation Results

The actual evapotranspiration (ETa) showed a consistent decline with increasing irrigation-water salinity, as shown in Fig. 10. Observed values decreased from 3.50 mm day^{-1} (I0) to 2.55 mm day^{-1} (I4), a trend that was closely reproduced by the model. Simulated ETa followed the same pattern, although with a systematic underestimation across treatments, particularly under higher salinity levels. The AquaCrop model demonstrated moderate performance in simulating ETa during the validation phase, with R^2 values ranging from 0.51 to 0.68. Higher agreement under non-saline conditions (I0; R^2 = 0.68) and lower values under saline treatments (I1–I4; R^2 = 0.51–0.58) indicate increased variability in ETa responses under stress conditions. The consistent underes-timation, supported by regression slopes below unity (0.58–0.88), highlights a sys-tematic deviation between simulated and observed values.

3.2. Irrigation Salinity Management Scenarios

The irrigation scenarios (Sc1–Sc5) and irrigation-water salinity levels (I0–I6), as defined in Section 2.2, represent increasing irrigation intensity and salinity levels, respectively. Simulation results under these conditions, combined with contrasting climatic periods (1996–2007 and 2018–2023), are presented in Fig. 11. Under dry conditions (Fig. 11A–C), grain yield (GY) decreased markedly with increasing irrigation-water salinity, declining from about 6.2 t ha^{-1} under low salinity to around 4.1 t ha^{-1} under high salinity. Biomass (B) showed a similar decline, while soil electrical conductivity (ECe) increased to approximately 10.3 dS m^{-1}. The reduction in GY and B became more pronounced beyond the threshold of approximately 7.0 dS m^{-1}. Under normal climatic conditions (Fig. 11D–F), GY remained higher, ranging from approximately 6.6 t ha^{-1} under low salinity to about 4.5 t ha^{-1} under high salinity. Biomass followed the same trend, while ECe increased with salinity and irrigation intensity, reaching values in the range of 9.8–11.2 dS m^{-1}. Under wet climatic conditions (Fig. 11G–I), GY reached its highest values, around 7.6 t ha^{-1} under low salinity, and decreased to

approximately 4.6 t ha^{-1} under higher salinity. Biomass showed a similar response, whereas ECe increased further, reaching approximately 11.5–13.2 dS m^{-1} under high salinity and irrigation intensity.

1. **Correlation of grain yield, total biomass, and soil salinity with saline irrigation treatments based on irrigation scenarios**

Figure 12 presents a heat map illustrating the combined effects of irrigation-water salinity levels (I0–I6) and irrigation intensity scenarios (Sc1–Sc5) on grain yield (GY), biomass (B), and soil electrical conductivity (ECe) over long-term climatic conditions. The visualization highlights clear gradients in crop performance and soil salinity, allowing a direct comparison of management responses under varying salinity and irrigation regimes. Across all irrigation scenarios, GY and B show a consistent decline along the salinity gradient, while ECe increases progressively, reflecting cumulative salt accumulation in the soil profile. At low to moderate salinity levels (up to approximately 7 dS m^{-1}), yield and biomass reductions remain limited, particularly under low to intermediate irrigation intensities (Sc1–Sc3), indicating a zone of relative stability in crop response. As salinity increases beyond this threshold, the heat map reveals a pronounced shift toward lower GY and B values, especially under higher irrigation intensities (Sc4 and Sc5). This pattern indicates that intensive irrigation amplifies the negative impact of salinity on crop productivity, rather than mitigating salt stress. In parallel, ECe values increase sharply under these scenarios, demonstrating accelerated soil salinization under combined high salinity and high irrigation input. The contrast between irrigation scenarios is particularly evident: Sc1 and Sc2 maintain comparatively higher yields and lower ECe values across most salinity levels, whereas Sc3, Sc4, and Sc5 display steeper gradients, highlighting greater sensitivity of both crop performance and soil salinity to management intensity.

3.4. Impact of Saline Irrigation on Soil Profile Moisture and Salinity

Figure 13 illustrates the vertical distribution of soil water content (SWC) and soil electrical conductivity (ECe) under the five saline irrigation treatments (I0–I4) across the 0–90 cm soil profile. Clear and contrasting patterns were observed for SWC and ECe, highlighting the combined effects of saline irrigation on soil moisture availability and salt accumulation within the root zone. Soil water content exhibited a consistent decreasing trend with increasing irrigation-water salinity, with the most pronounced reductions occurring in the upper soil layers. In the 0–30 cm layer, SWC declined from 46.8% under the control treatment (I0) to 33.8% under the highest salinity treatment (I4), indicating a strong limitation of water availability in the most biologically active soil horizon. In contrast, deeper layers (60–90 cm) showed comparatively smaller variations, with SWC values ranging from 42.0% to 30.8%, suggesting a buffering effect at depth. Across the entire profile, mean SWC decreased progressively from 43.4% (I0) to 32.0% (I4), reflecting the cumulative impact of salinity on soil water retention. Soil salinity displayed an opposite vertical pattern. The highest ECe values were systematically recorded in the surface layers, increasing sharply from 1.4 dS m^{-1} under I0 to 10.5 dS m^{-1} under I4, indicating strong salt accumulation near the soil surface due to evaporation and limited leaching. With increasing depth, ECe gradually decreased, reaching values between 0.7 and 5.6 dS m^{-1} at 90 cm. Average profile salinity increased steadily across treatments, from 1.0 dS m^{-1} under I0 to 7.9 dS m^{-1} under I4.

4. Discussion

The performance of the AquaCrop model under saline irrigation conditions in the Tadla plain demonstrates its strong ability to capture the key soil–plant interactions governing crop responses to osmotic and ionic stress. Canopy cover (CC) simulations showed that AquaCrop accurately reproduced the seasonal development of winter wheat canopies across all salinity treatments. The high coefficients of determination (R^2 = 0.99), together with very low RMSE and NRMSE values, confirm that the model effectively captured both the magnitude and the temporal dynamics of canopy expansion and senescence. This strong performance indicates that the calibrated canopy growth coefficient (CGC) and

canopy decline coefficient (CDC) parameters reliably represented the physiological response of wheat under saline irrigation, where osmotic stress limits leaf expansion and accelerates canopy senescence. Consistent with field observations, the model successfully reproduced the progressive reduction in canopy cover from approximately 65% under non-saline conditions to about 39% under the highest salinity level, reflecting the inhibitory effects of salinity on vegetative development. These results are in agreement with previous studies. For instance, after parameterizing the canopy cover curve based on leaf area index (LAI) observations, AquaCrop accurately simulated canopy dynamics of vining pea, with RMSE values below 15% of ground cover [67]. Similarly, Jallal et al., 2025 [68] reported that AquaCrop, once calibrated for canopy growth parameters, precisely reproduced canopy development of pea crops under semi-arid conditions, demonstrating the robustness of the model for simulating leaf growth under variable water availability.

The slight tendency of AquaCrop to underestimate canopy cover in some treatments, as indicated by negative percent error values, remains within an acceptable modelling range. Comparable deviations have been reported in canopy simulations under water and salinity stress, where process-based models may underestimate canopy development during periods of accelerated senescence or increased spatial variability [49–51]. Furthermore, recent evaluations under saline and arid environments reported early- and mid-season discrepancies between simulated and observed canopy cover, suggesting that such deviations are characteristic of crop models operating under fluctuating environmental constraints rather than structural model deficiencies [70].

Simulated grain yield (GY) and biomass (B) declined progressively with increasing irrigation-water salinity, reaching reductions of up to 40% at 10 dS m^{-1}. This response follows the classical two-segment salt–yield relationship described [71], in which crop yield remains relatively stable up to a threshold salinity level and subsequently decreases in a near-linear manner. Beyond this threshold, osmotic constraints and ionic toxicity reduce root water uptake, disrupt photosynthetic processes, and limit assimilate allocation to reproductive organs. Recent advances in salt-stress physiology indicate that salinity perturbs cellular homeostasis and activates stress-responsive metabolic pathways, ultimately restricting biomass accumulation [72–74].Salt stress has been shown to compromise chloroplast integrity by altering lamellar organization and impairing the photosynthetic apparatus, thereby reducing carbon assimilation and reinforcing yield losses under high salinity conditions. In this study, AquaCrop implicitly reproduced these physiological constraints by simulating reduced canopy expansion and accelerated canopy decline under increasing salinity. This modelling behavior is consistent with experimental evidence showing that elevated salinity induces oxidative stress and inhibits photosynthetic activity [75, 76]. The strong agreement between simulated canopy dynamics and physiological responses reported in controlled and field studies further supports the robustness of the calibrated model parameters [76–78]. Importantly, the results indicate that crop performance remained relatively stable up to moderate salinity levels, while a marked decline occurred at higher salinity, reinforcing the existence of a tolerance threshold.

The identification of a performance threshold close to 7 dS m^{-1}, beyond which yield reductions became pronounced, is in agreement with wheat tolerance studies reporting accelerated yield decline at elevated salinity due to disruptions in ion homeostasis, oxidative stress, and impaired photosynthetic capacity [80]. Field-based screening of diverse wheat accessions under saline conditions has also revealed substantial genotypic variation in growth and yield responses, highlighting cultivar-specific buffering capacity against salt stress [81]. Overall, the consistent decline in productivity across increasing salinity levels reflects integrated biophysical limitations, including reduced transpiration efficiency, impaired nutrient uptake, and altered biomass partitioning [82–84]. These mechanisms provide a coherent explanation for the parallel decrease in both TDM and GY observed in this study and emphasize the vulnerability of wheat-based cropping systems irrigated with saline water.

AquaCrop accurately reproduced soil water content (SWC) dynamics across salinity treatments during both the calibration (2023) and validation (2022) seasons. Coefficients of determination ranged from 0.85 to 0.91, while NRMSE values remained within 8–10%, indicating good temporal agreement between simulated and observed soil moisture

under independent climatic conditions. These results demonstrate the model's capacity to represent key hydrological processes, including soil evaporation, root water uptake, and salinity-induced limitations on water availability. A slight overestimation of SWC was observed under the highest salinity treatments, particularly during the validation season, which is consistent with previous studies reporting a tendency of AquaCrop to overpredict soil moisture under saline conditions [85–87]. This behavior is commonly attributed to the simplified representation of soil structural heterogeneity and solute transport processes, which can influence water retention and redistribution under elevated salt concentrations. Despite these minor deviations, model performance remained stable across years, confirming that AquaCrop provides a robust and transferable framework for simulating soil moisture dynamics under combined water and salinity stress.

The simulation of actual evapotranspiration (ETa) showed moderate but consistent accuracy across both the calibration and validation seasons. AquaCrop successfully reproduced the overall decline in ETa with increasing irrigation-water salinity, reflecting the progressive limitation of crop water use under saline conditions, although short-term fluctuations were only partially captured. This level of performance is consistent with previous AquaCrop applications reported for legumes [88], soybean [89], and chickpea under semi-arid environments [90], where the model effectively represented seasonal ETa trends while smoothing daily variability. In the present study, a slight overestimation of ETa under higher salinity levels was observed, particularly during the validation season, which is consistent with known simplifications in AquaCrop's osmotic stress functions that may not fully capture rapid reductions in stomatal conductance under severe salt stress. Additional discrepancies may also arise from the contrast between the homogeneous simulation domain assumed by the model and the spatial heterogeneity of field-based ETa measurements, an issue previously highlighted in Moroccan winter wheat systems [91]. Moreover, these discrepancies are closely linked to irrigation management, as previous studies have shown that although saline irrigation may temporarily alleviate water deficits, excessive water application accelerates soil salinity buildup, thereby indirectly affecting crop water uptake and evapotranspiration dynamics [92–94].

Moreover, irrigation practices under saline conditions introduce additional feedback mechanisms. While irrigation may temporarily sustain evapotranspiration, it can also promote salt accumulation in the root zone, which restricts plant water uptake and alters ETa dynamics over time. These interactions between irrigation, salinity, and crop water use are difficult to fully capture using simplified modeling approaches and have been identified as key challenges in saline environments [92–94]. This limitation is consistent with the conceptual design of AquaCrop, which prioritizes robustness and simplicity over detailed representation of complex physiological and soil processes. Despite these constraints, the moderate performance of ETa simulations did not significantly affect the accuracy of biomass (B) and grain yield (GY) predictions. This is because AquaCrop links biomass production primarily to cumulative transpiration rather than daily ETa dynamics. Consequently, even if short-term fluctuations are not fully captured, the model remains capable of providing reliable estimates of seasonal crop productivity under saline conditions.

The relationship between evapotranspiration (ETa), biomass production, and grain yield is a fundamental component of the AquaCrop modeling framework [38, 39, 95]. In this model, biomass is driven by crop transpiration through normalized water productivity (WP), while grain yield is subsequently determined by the harvest index (HI). In this context, uncertainties in ETa may propagate to biomass and ultimately to grain yield. However, in the present study, ETa showed moderate agreement with observed values (R^2 ranging from 0.47 to 0.65 during calibration and from 0.51 to 0.68 during validation), whereas biomass and grain yield were simulated with high accuracy (R^2 up to 0.85 and 0.98 during calibration and remaining above 0.80 and 0.92 during validation, respectively, with NRMSE below 4%). Despite an approximate 29% reduction in ETa under highsalinity conditions, the model accurately reproduced the corresponding decrease in biomass and grain yield across treatments. This comparison indicates that ETa uncertainty, although relatively high, results in only minor errors in grain yield prediction (NRMSE < 4%), demonstrating a limited propagation of ETa uncertainty to seasonal yield. This reflects an attenuation of uncertainty from ETa to yield at the seasonal scale.

This behavior can be explained by the model structure, where biomass depends on cumulative transpiration rather than instantaneous ETa values, and the harvest index (HI) acts as a regulating factor that buffers the effect of ETa variability on final yield estimation [96].

Simulated soil electrical conductivity (ECe) displayed clear vertical gradients, increasing from approximately 1–2 dS m^{-1} under low-salinity irrigation to 13–14.5 dS m^{-1} under highly saline conditions. This pattern reflects limited salt leaching under semi-arid conditions combined with strong evaporative fluxes, which promote salt accumulation in the upper soil layer [97]. The satisfactory model performance, with coefficients of determination (R^2) ranging from 0.70 to 0.80 across calibration and validation periods, indicates that AquaCrop, despite its simplified salinity module, effectively captures the dominant processes driving soil salinization [98]. These results are consistent with previous studies showing that effective root depth (Zx) and canopy development play a key role in controlling vertical salt redistribution within the soil profile. They also align with field-based evaluations reporting strong correlations between simulated and observed soil salinity patterns, particularly under saline irrigation regimes.

5. Conclusion

This study demonstrates the value of the AquaCrop model as a reliable decision-support tool for managing saline irrigation of winter wheat under semi-arid Moroccan conditions. The model was successfully calibrated (2023) and independently validated (2022), accurately reproducing key crop and soil processes, including canopy development, soil water content, evapotranspiration, biomass, yield, and soil salinity dynamics, confirming the robustness of the calibrated parameters for the Achtar variety. The results revealed a clear threshold response to salinity, with crop productivity remaining stable under low to moderate salinity and declining sharply beyond approximately 7 dS m^{-1}. Scenario analysis showed that moderate irrigation strategies maintained yield while limiting salt accumulation, whereas higher irrigation inputs accelerated soil salinization without improving productivity. Overall, this research highlights the importance of optimizing irrigation strategies when using saline water and confirms the potential of AquaCrop as a valuable tool for operational irrigation planning in semi-arid regions. Future work should include additional field validation and integrate economic and environmental assessments to support sustainable water management.

Additional Information

Declarations

Conflict of interest:

The Authors state they have no known conflicting financial interests or personal relationships that would appear to affect the work reported in this manuscript.

Ethical approval:

Not applicable.

Consent to participate:

Not applicable.

Consent to publish:

All authors have reviewed and approved the submission and publication of this manuscript.

Funding:

This research did not receive any specific grant from funding agencies in the public, commercial, or not-for-profit sectors.

Author contributions

Khadija Manhou: Writing – original draft, Writing – review & editing, Visualization, Validation, Software, Resources, Methodology, Formal analysis, Conceptualization. **Rachid Moussadek**: Writing – review & editing, Formal analysis. **Abdelmjid Zouahri**: Writing – original draft, Writing – review & editing, Validation, Supervision. **Zoubida Belmahi**: Writing – review & editing, Resources. **Ahmed Ghanimi**: Writing – review & editing, Resources, Methodology. **Majda Oueld Lhaj**: Writing – review & editing, Resources. **Hatim Sanad**: Writing – review & editing, Resources. **Driss Hmouni**: Writing – original draft, Writing – review & editing, Validation, Supervision. **Houria Dakak**: Writing – original draft, Writing – review & editing, Validation, Supervision, Methodology.

Acknowledgements

The authors extend their gratitude to all collaborators involved in field sampling,laboratory anal-ysis, and manuscript preparation. The authors also acknowledge the financial supportprovided by the “MCGP INRA-ICARDA” and “EiA” projects.

Data Availability:

The data is available on request from the corresponding author.

References

1. Manhou K, Moussadek R, Yachou H, Zouahri A, Douaik A, Hilal I, Ghanimi A, Hmouni D, Dakak H (2024) Assessing the Impact of Saline Irrigation Water on Durum Wheat (Cv. Faraj) Grown on Sandy and Clay Soils. Agronomy 14:2865. 10.3390/agronomy14122865
2. Tarolli P, Luo J, Park E, Barcaccia G, Masin R (2024) Soil Salinization in Agriculture: Mitigation and Adaptation Strategies Combining Nature-Based Solutions and Bioengineering. *iScience 27*, 108830. 10.1016/j.isci.2024.108830
3. Steduto P (2012) *Coping with Water Scarcity: An Action Framework for Agriculture and Food Security*; FAO water reports; FAO: Rome, ; ISBN 978-92-5-107304-9
4. Hamad A, Tayel A Food 2050 Concept: Trends That Shape the Future of Food. J Future Foods 2025, S2772566925001260, 10.1016/j.jfutfo.2025.03.003
5. Dotaniya ML, Meena VD, Saha JK, Dotaniya CK, Mahmoud AED, Meena BL, Meena MD, Sanwal RC, Meena RS, Doutaniya RK et al (2023) Reuse of Poor-Quality Water for Sustainable Crop Production in the Changing Scenario of Climate. Environ Dev Sustain 25:7345–7376. 10.1007/s10668-022-02365-9
6. Qadir M, Quillérou E, Nangia V, Murtaza G, Singh M, Thomas RJ, Drechsel P, Noble AD (2014) Economics of Salt-induced Land Degradation and Restoration. Nat Resour Forum 38:282–295. 10.1111/1477-8947.12054

7. Sanad H, Moussadek R, Mouhir L, Zouahri A, Oueld Lhaj M, Monsif Y, Manhou K, Dakak H (2026) Artificial Intelligence (AI) and Monte Carlo Simulation-Based Modeling for Predicting Groundwater Pollution Indices and Nitrate-Linked Health Risks in Coastal Areas Facing Agricultural Intensification. Hydrology 13:59. 10.3390/hydrology13020059
8. Lian T, Cheng L, Liu Q, Yu T, Cai Z, Nian H, Hartmann M (2023) Potential Relevance between Soybean Nitrogen Uptake and Rhizosphere Prokaryotic Communities under Waterlogging Stress. ISME Commun 3:71. 10.1038/s43705-023-00282-0
9. Rathore VS, Nathawat NS, Bhardwaj S, Sasidharan RP, Yadav BM, Kumar M, Santra P, Yadava ND, Yadav OP, Yield (2017) Water and Nitrogen Use Efficiencies of Sprinkler Irrigated Wheat Grown under Different Irrigation and Nitrogen Levels in an Arid Region. Agric Water Manage 187:232–245. 10.1016/j.agwat.2017.03.031
10. Blil N, Sahbani Z, Manhou K, Boumalik D, Guessous Z Beyond Phragmites and Typha: A Global Bibliometric Analysis and Strategic Selection of Pioneer Macrophytes for Wastewater Treatment 2025
11. El Sabagh A, Islam MS, Skalicky M, Ali Raza M, Singh K, Anwar Hossain M, Hossain A, Mahboob W, Iqbal MA, Ratnasekera D et al (2021) Salinity Stress in Wheat (Triticum Aestivum L.) in the Changing Climate: Adaptation and Management Strategies. Front Agron 3:661932. 10.3389/fagro.2021.661932
12. Si Z, Qin A, Liang Y, Duan A, Gao Y (2023) A Review on Regulation of Irrigation Management on Wheat Physiology, Grain Yield, and Quality. *Plants 12*, 692. 10.3390/plants12040692
13. Manhou K, Moussadek R, Zouahri A, Ghanimi A, Sanad H, Oueld Lhaj M, Hmouni D, Dakak H, Performance (2025) Agro-Morphological, and Quality Traits of Durum Wheat (Triticum Turgidum L. Ssp. Durum Desf.) Germplasm: A Case Study in Jemâa Shaïm, Morocco. *Plants 14*, 1508. 10.3390/plants14101508
14. Oueld Lhaj M, Moussadek R, Sanad H, Zouahri A, Manhou K, Alaoui MM, Mouhir L (2026) Compost Improves Soil Fertility Index and Tomato (Lycopersicon Esculentum L.) Yield under Drought: Integrating Multivariate Soil–Plant Modeling and Monte Carlo Simulation across Sandy Loam and Silty Clay Soils. Front Sustain Food Syst 10:1797471. 10.3389/fsufs.2026.1797471
15. Machado R, Serralheiro R, Soil Salinity (2017) Effect on Vegetable Crop Growth. Management Practices to Prevent and Mitigate Soil Salinization. Horticulturae 3:30. 10.3390/horticulturae3020030
16. Manhou K, Moussadek R, Dakak H, Zouahri A, Ghanimi A, Sanad H, Oueld Lhaj M, Hmouni D (2025) Effect of Irrigation with Saline Water on Germination, Physiology, Growth, and Yield of Durum Wheat Varieties on Silty Clay Soil. Agriculture 15:2364. 10.3390/agriculture15222364
17. Oueld Lhaj M, Moussadek R, Mouhir L, Sanad H, Manhou K, Iben Halima O, Yachou H, Zouahri A, Mdarhri Alaoui M (2025) Application of Compost as an Organic Amendment for Enhancing Soil Quality and Sweet Basil (Ocimum Basilicum L.) Growth: Agronomic and Ecotoxicological Evaluation. Agronomy 15:1045. 10.3390/agronomy15051045
18. Solgi S, Ahmadi SH, Sepaskhah AR, Edalat M (2022) Wheat Yield Modeling under Water-Saving Irrigation and Climatic Scenarios in Transition from Surface to Sprinkler Irrigation Systems. J Hydrol 612:128053. 10.1016/j.jhydrol.2022.128053
19. Jiang Y, Wang X, Ti J, Lu Z, Yin X, Chu Q, Lei Y, Chen F (2020) Assessment of Winter Wheat Water-saving Potential in the Groundwater Overexploitation District of the North China Plain. Agron J 112:44–55. 10.1002/agj2.20041
20. Seleiman F, Talha Aslam M, Ahmed Alhammad M, Umair Hassan B, Maqbool M, Umer Chattha R, Khan M, Ireri I, Gitari H, Uslu S, Roy O et al (2022) R.;. Salinity Stress in Wheat: Effects, Mechanisms and Management Strategies. *Phyton 91*, 667–694. 10.32604/phyton.2022.017365
21. Mosaffa HR, Sepaskhah AR (2019) Performance of Irrigation Regimes and Water Salinity on Winter Wheat as Influenced by Planting Methods. Agric Water Manage 216:444–456. 10.1016/j.agwat.2018.10.027

22. Manhou K, Hmouni D, Moussadek R, Zouahri A, Yachou H, Lhaj MO, Sanad H, Ghanimi A, Dakak H (2026) Compost Application Enhances Soil Quality, Growth, and Yield of Durum Wheat under Saline Conditions. Sci Rep 16:7643. 10.1038/s41598-026-36306-7
23. Huang M, Zhang Z, Zhai Y, Lu P, Zhu C (2019) Effect of Straw Biochar on Soil Properties and Wheat Production under Saline Water Irrigation. Agronomy 9:457. 10.3390/agronomy9080457
24. Sanad H, Moussadek R, Mouhir L, Lhaj MO, Dakak H, Manhou K, Zouahri A (2025) Monte Carlo Simulation for Evaluating Spatial Dynamics of Toxic Metals and Potential Health Hazards in Sebou Basin Surface Water. Sci Rep 15:29471. 10.1038/s41598-025-15006-8
25. Wang X, Yang J, Liu G, Yao R, Yu S (2015) Impact of Irrigation Volume and Water Salinity on Winter Wheat Productivity and Soil Salinity Distribution. Agric Water Manage 149:44–54. 10.1016/j.agwat.2014.10.027
26. Zhai Y, Huang M, Zhu C, Xu H, Zhang Z (2022) Evaluation and Application of the AquaCrop Model in Simulating Soil Salinity and Winter Wheat Yield under Saline Water Irrigation. Agronomy 12:2313. 10.3390/agronomy12102313
27. Du T, Kang S, Zhang J, Davies WJ (2015) Deficit Irrigation and Sustainable Water-Resource Strategies in Agriculture for China's Food Security. J Exp Bot 66:2253–2269. 10.1093/jxb/erv034
28. Sanad H, Moussadek R, Mouhir L, Lhaj MO, Zahidi K, Dakak H, Manhou K, Zouahri A (2025) Ecological and Human Health Hazards Evaluation of Toxic Metal Contamination in Agricultural Lands Using Multi-Index and Geostatistical Techniques across the Mnasra Area of Morocco's Gharb Plain Region. J Hazard Mater Adv 18:100724. 10.1016/j.hazadv.2025.100724
29. Shoukat Hafiza B, Ishaque W, Ahmad S, Ali S, El-Sheikh MA (2025) Optimizing Wheat Productivity and Water Productivity through Deficit Irrigation Strategies in Semi-Arid Environments. Sci Rep 15:20630. 10.1038/s41598-025-04618-9
30. Yuan H, Zhang A, Zhu C, Dang H, Zheng C, Zhang J, Cao C (2024) Saline Water Irrigation Changed the Stability of Soil Aggregates and Crop Yields in a Winter Wheat–Summer Maize Rotation System. *Agronomy 14*, 2564. 10.3390/agronomy14112564
31. Vanuytrecht E, Raes D, Steduto P, Hsiao TC, Fereres E, Heng LK, Garcia Vila M (2014) Mejias Moreno, P. AquaCrop: FAO's Crop Water Productivity and Yield Response Model. Environ Model Softw 62:351–360. 10.1016/j.envsoft.2014.08.005
32. Feng Z, Miao Q, Shi H, Gonçalves JM, Li X, Feng W, Yan J, Yu D, Yan Y (2025) AquaCrop Model-Based Sensitivity Analysis of Soil Salinity Dynamics and Productivity under Climate Change in Sandy-Layered Farmland. Agric Water Manage 307:109244. 10.1016/j.agwat.2024.109244
33. Zhai Y, Huang M, Zhu C, Xu H, Zhang Z (2022) Evaluation and Application of the AquaCrop Model in Simulating Soil Salinity and Winter Wheat Yield under Saline Water Irrigation. Agronomy 12:2313. 10.3390/agronomy12102313
34. Liu B, Wang S, Kong X, Liu X, Sun H (2019) Modeling and Assessing Feasibility of Long-Term Brackish Water Irrigation in Vertically Homogeneous and Heterogeneous Cultivated Lowland in the North China Plain. Agric Water Manage 211:98–110. 10.1016/j.agwat.2018.09.030
35. Soothar RK, Wang C, Li L, Cui N, Zhang W, Wang Y (2021) Soil Salt Accumulation, Physiological Responses, and Yield Simulation of Winter Wheat to Alternate Saline and Fresh Water Irrigation in the North China Plain. J Soil Sci Plant Nutr 21:2072–2082. 10.1007/s42729-021-00503-2
36. Rasouli F, Kiani Pouya A, Šimůnek J (2013) Modeling the Effects of Saline Water Use in Wheat-Cultivated Lands Using the UNSATCHEM Model. Irrig Sci 31:1009–1024. 10.1007/s00271-012-0383-8
37. Kumar P, Sarangi A, Singh DK, Parihar SS, Sahoo RN (2015) Simulation of Salt Dynamics in the Root Zone and Yield of Wheat Crop under Irrigated Saline Regimes Using SWAP Model. Agric Water Manage 148:72–83. 10.1016/j.agwat.2014.09.014

38. Raes D, Steduto P, Hsiao TC, Fereres E, AquaCrop (2009) — The FAO Crop Model to Simulate Yield Response to Water: II. Main Algorithms and Software Description. *Agronomy Journal 101*, 438–447. 10.2134/agronj2008.0140s
39. Steduto P, Hsiao TC, Raes D, Fereres E, AquaCrop—The (2009) FAO Crop Model to Simulate Yield Response to Water: I. Concepts and Underlying Principles. Agron J 101:426–437. 10.2134/agronj2008.0139s
40. Farahani HJ, Izzi G, Oweis TY (2009) Parameterization and Evaluation of the AquaCrop Model for Full and Deficit Irrigated Cotton. Agron J 101:469–476. 10.2134/agronj2008.0182s
41. García-Vila M, Fereres E (2012) Combining the Simulation Crop Model AquaCrop with an Economic Model for the Optimization of Irrigation Management at Farm Level. Eur J Agron 36:21–31. 10.1016/j.eja.2011.08.003
42. Xiangxiang W, Quanjiu W, Jun F, Qiuping F (2013) Evaluation of the AquaCrop Model for Simulating the Impact of Water Deficits and Different Irrigation Regimes on the Biomass and Yield of Winter Wheat Grown on China's Loess Plateau. Agric Water Manage 129:95–104. 10.1016/j.agwat.2013.07.010
43. El Kiram N, Jaffal M, Kchikach A, El Azzab D, El Ghorfi M, Khadiri O, Jourani E-S, Manar A, Nahim M (2019) Phosphatic Series under Plio-Quaternary Cover of Tadla Plain, Morocco: Gravity and Seismic Data. Comptes Rendus Géoscience 351:420–429. 10.1016/j.crte.2019.05.002
44. Didi S, Housni FE, Del Bracamontes H, Najine A (2019) Mapping of Soil Salinity Using the Landsat 8 Image and Direct Field Measurements: A Case Study of the Tadla Plain, Morocco. J Indian Soc Remote Sens 47:1235–1243. 10.1007/s12524-019-00979-7
45. Salahddine D, Housni FE, Najine A, Wafik A, Aadraoui M, Hafiane FZ, Del Toro HB (2017) Mapping and Characterization of Agricultural Systems from Time Series of Normalized Difference Vegetation Index (NDVI) in the Northeast Area of Tadla, Morocco. *NR 08*, 24–30. 10.4236/nr.2017.81002
46. Barakat A, Ennaji W, El Jazouli A, Amediaz R, Touhami F (2017) Multivariate Analysis and GIS-Based Soil Suitability Diagnosis for Sustainable Intensive Agriculture in Beni-Moussa Irrigated Subperimeter (Tadla Plain, Morocco). Model Earth Syst Environ 3(3). 10.1007/s40808-017-0272-5
47. Aghzar N, Berdai H, Bellouti A, Soudi B (2005) Ground Water Nitrate Pollution in Tadla (Morocco). *rseau 15*, 459–492. 10.7202/705465ar
48. Oweis T, Hachum A (2009) Optimizing Supplemental Irrigation: Tradeoffs between Profitability and Sustainability. Agric Water Manage 96:511–516. 10.1016/j.agwat.2008.09.029
49. Allen RG, Pereira LS, Raes D, Smith M (1998) Crop Evapotranspiration-Guidelines for Computing Crop Water Requirements-FAO Irrigation and Drainage Paper 56. *Fao, rome 300*, D05109
50. NASA LaRC NASA POWER Data Access Viewer 2022
51. Bouyoucos GJ (1962) Hydrometer Method Improved for Making Particle Size Analyses of Soils [1]. Agron J 54:464–465. 10.2134/agronj1962.00021962005400050028x
52. Rowell DL (2014) *Soil Science: Methods & Applications*; Routledge: London, UK, ; ISBN 978-1-315-84485-5
53. Methods of Soil Analysis (1983) Part 2 Chemical and Microbiological Properties. Page L
54. Van Reeuwijk LP (1986) Procedures for Soil Analysis. Technical Paper, International Soil Reference and Information Centre: Wageningen, The Netherlands,
55. Jackson ML (1958) *Soil Chemical Analysis: Advanced Course: A Manual of Methods Useful for Instruction and Research in Soil Chemistry, Physical Chemistry of Soils, Soil Fertility, and Soil Genesis*; UW-Madison Libraries Parallel Press: London, UK, ; ISBN 978-1-893311-47-3
56. Baruah TC, Barthakur HP (1997) A Textbook of Soil Analysis. Vikas Publishing House PVT Ltd., New Delhi, India
57. Soil Survey Staff *Soil Taxonomy: A Basic System of Soil Classification for Making and Interpreting Soil Surveys*; 2nd ed.; USDA Natural Resources Conservation Service: Washington, DC, (1999)

58. *Guidelines for Drinking-Water Quality*; World Health Organization, Ed.; Fourth edition incorporating the first addendum.; World Health Organization: Geneva, 2017; ISBN 978-92-4-154995-0
59. Hsiao TC, Heng L, Steduto P, Rojas-Lara B, Raes D, Fereres E (2009) AquaCrop—The FAO Crop Model to Simulate Yield Response to Water: III. Parameterization and Testing for Maize. Agron J 101:448–459. 10.2134/agronj2008.0218s
60. Vanuytrecht E, Raes D, Steduto P, Hsiao TC, Fereres E, Heng LK, Garcia Vila M (2014) Mejias Moreno, P. AquaCrop: FAO's Crop Water Productivity and Yield Response Model. Environ Model Softw 62:351–360. 10.1016/j.envsoft.2014.08.005
61. Trucano TG, Swiler LP, Igusa T, Oberkampf WL, Pilch M, Calibration (2006) Validation, and Sensitivity Analysis: What's What. Reliab Eng Syst Saf 91:1331–1357. 10.1016/j.ress.2005.11.031
62. Sargent RG (2010) Verification and Validation of Simulation Models. In Proceedings of the Proceedings of the 2010 Winter Simulation Conference; IEEE: Baltimore, MD, USA, December ; pp. 166–183
63. Jacovides CP, Kontoyiannis H (1995) Statistical Procedures for the Evaluation of Evapotranspiration Computing Models. Agric Water Manage 27:365–371. 10.1016/0378-3774(95)01152-9
64. Jamieson PD, Porter JR, Wilson DR (1991) A Test of the Computer Simulation Model ARCWHEAT1 on Wheat Crops Grown in New Zealand. Field Crops Res 27:337–350. 10.1016/0378-4290(91)90040-3
65. Feng Z, Miao Q, Shi H, Li X, Yan J, Gonçalves JM, Dai L, Feng W (2024) Irrigation Scheduling in Sand-Layered Farmland: Evaluation of Water and Salinity Dynamics in the Soil by SALTMED-1D Model under Mulched Maize Production in Hetao Irrigation District, China. Eur J Agron 157:127177. 10.1016/j.eja.2024.127177
66. Liu M, Shi H, Paredes P, Ramos TB, Dai L, Feng Z, Pereira LS (2022) Estimating and Partitioning Maize Evapotranspiration as Affected by Salinity Using Weighing Lysimeters and the SIMDualKc Model. Agric Water Manage 261:107362. 10.1016/j.agwat.2021.107362
67. Khorsand A, Dehghanisanij H, Heris AM, Asgarzadeh H, Rezaverdinejad V (2024) Calibration and Evaluation of the FAO AquaCrop Model for Canola (Brassica Napus) under Full and Deficit Irrigation in a Semi-Arid Region. Appl Water Sci 14:56. 10.1007/s13201-024-02108-3
68. Jallal L, Er-Raki S, Khabba S, Ezzahar J, Kaissi O, Rafi Z, Chehbouni A (2025) Simulation of the Pea Crop Development Using AquaCrop Model in Chichaoua Region, Morocco: Application for Irrigation Management. Agric Water Manage 322:109943. 10.1016/j.agwat.2025.109943
69. Dhouib M, Zitouna-Chebbi R, Prévot L, Molénat J, Mekki I, Jacob F (2022) Multicriteria Evaluation of the AquaCrop Crop Model in a Hilly Rainfed Mediterranean Agrosystem. Agric Water Manage 273:107912. 10.1016/j.agwat.2022.107912
70. Sekhri L, Razi S, Merdaci S, Sellem F, Daibouche Y, Poddubsky A, Kucher DE, Rebouh NY, Fadl ME (2025) Accurate Prediction of Wheat Yield under Combined Saline Water Irrigation and Arid Stress: A Comprehensive Analysis of the FAO-AquaCrop Model. Front Sustain Food Syst 9:1709629. 10.3389/fsufs.2025.1709629
71. Maas EV, Grattan SR (1999) Crop Yields as Affected by Salinity. In *Agronomy Monographs*; Skaggs, R.W., Schilfgaarde, J., Eds.; Wiley, ; Vol. 38, pp. 55–108 ISBN 978-0-89118-141-5
72. Hameed A, Ahmed MZ, Hussain T, Aziz I, Ahmad N, Gul B, Nielsen BL (2021) Effects of Salinity Stress on Chloroplast Structure and Function. *Cells 10*, 2023. 10.3390/cells10082023
73. Sanad H, Moussadek R, Zouahri A, Lhaj MO, Mouhir L, Dakak H (2025) Machine Learning-Integrated Hydrogeochemical and Spatial Modeling of Groundwater Quality Indices for Seawater Intrusion and Irrigation Sustainability in Coastal Agroecosystems of Skhirat Region, Morocco. J Hydrology: Reg Stud 62:102848. 10.1016/j.ejrh.2025.102848

74. Zhou H, Shi H, Yang Y, Feng X, Chen X, Xiao F, Lin H, Guo Y (2023) Insights into Plant Salt Stress Signaling and Tolerance. J Genet Genomics 51:16–34. 10.1016/j.jgg.2023.08.007
75. Atta K, Mondal S, Gorai S, Singh AP, Kumari A, Ghosh T, Roy A, Hembram S, Gaikwad DJ, Mondal S et al (2023) Impacts of Salinity Stress on Crop Plants: Improving Salt Tolerance through Genetic and Molecular Dissection. Front Plant Sci 14:1241736. 10.3389/fpls.2023.1241736
76. Patwa N, Pandey V, Gupta OP, Yadav A, Meena MR, Ram S, Singh G (2024) Unravelling Wheat Genotypic Responses: Insights into Salinity Stress Tolerance in Relation to Oxidative Stress, Antioxidant Mechanisms, Osmolyte Accumulation and Grain Quality Parameters. BMC Plant Biol 24:875. 10.1186/s12870-024-05508-4
77. Oueld Lhaj M, Moussadek R, Sanad H, Manhou K, Oueld Lhaj M, Mdarhri Alaoui M, Zouahri A, Mouhir L (2026) Ecological and Microbial Processes in Green Waste Co-Composting for Pathogen Control and Evaluation of Compost Quality Index (CQI) Toward Agricultural Biosafety. Environments 13:43. 10.3390/environments13010043
78. Zhai Y, Huang M, Zhu C, Xu H, Zhang Z (2022) Evaluation and Application of the AquaCrop Model in Simulating Soil Salinity and Winter Wheat Yield under Saline Water Irrigation. Agronomy 12:2313. 10.3390/agronomy12102313
79. Oueld Lhaj M, Moussadek R, Zouahri A, Sanad H, Saafadi L, Mdarhri Alaoui M, Mouhir L (2024) Sustainable Agriculture Through Agricultural Waste Management: A Comprehensive Review of Composting's Impact on Soil Health in Moroccan Agricultural Ecosystems. Agriculture 14:2356. 10.3390/agriculture14122356
80. Farooq M, Zahra N, Ullah A, Nadeem F, Rehman A, Kapoor R, Al-Hinani MS, Siddique KH (2024) M. Salt Stress in Wheat: Effects, Tolerance Mechanisms, and Management. J Soil Sci Plant Nutr 24:8151–8173. 10.1007/s42729-024-02104-1
81. Salim SA, Rasheed FT, Al-Deen UH, Almunem RA, Alalwany AAM (2024) Assessment of Salt Tolerance in Wheat Accessions: Growth and Yield Components under Saline Conditions. *AJSAT 13*, 40–44. 10.70112/ajsat-2024.13.2.4225
82. Hussein MAA, Alqahtani MM, Alwutayd KM, Aloufi AS, Osama O, Azab ES, Abdelsattar M, Hassanin AA, Okasha SA (2023) Exploring Salinity Tolerance Mechanisms in Diverse Wheat Genotypes Using Physiological, Anatomical, Agronomic and Gene Expression Analyses. *Plants 12*, 3330. 10.3390/plants12183330
83. Loudari A, Mayane A, Zeroual Y, Colinet G, Oukarroum A (2022) Photosynthetic Performance and Nutrient Uptake under Salt Stress: Differential Responses of Wheat Plants to Contrasting Phosphorus Forms and Rates. Front Plant Sci 13:1038672. 10.3389/fpls.2022.1038672
84. Mahboob W, Rizwan M, Irfan M, Hafeez OBA, Sarwar N, Akhtar M, Munir M, Rani R, Sabagh E, Shimelis A (2023) SALINITY TOLERANCE IN WHEAT: RESPONSES, MECHANISMS AND ADAPTATION APPROACHES. Appl Ecol Env Res 21:5299–5328. 10.15666/aeer/2106_52995328
85. Hammami Z, Qureshi AS, Sahli A, Gauffreteau A, Chamekh Z, Ben Azaiez FE, Ayadi S, Trifa Y (2020) Modeling the Effects of Irrigation Water Salinity on Growth, Yield and Water Productivity of Barley in Three Contrasted Environments. *Agronomy 10*, 1459. 10.3390/agronomy10101459
86. Sahbani Z, Blil N, Ouadi AE (2025) A Bibliometric Analysis of Research on Application of AI in Wastewater Treatment, 1987–2024
87. Hamdi L, Suleiman A (2024) Evaluating the Performance of the AquaCrop Model to Soil Salinity in Jordan Valley. Jordan j Agr sci. 10.35516/jjas.v20i2.2335
88. Paredes P, Torres MO (2017) Parameterization of AquaCrop Model for Vining Pea Biomass and Yield Predictions and Assessing Impacts of Irrigation Strategies Considering Various Sowing Dates. Irrig Sci 35:27–41. 10.1007/s00271-016-0520-x
89. Adeboye OB, Schultz B, Adeboye AP, Adekalu KO, Osunbitan JA (2021) Application of the AquaCrop Model in Decision Support for Optimization of Nitrogen Fertilizer and Water Productivity of Soybeans. Inform Process Agric

8:419–436. 10.1016/j.inpa.2020.10.002

90. Mubvuma MT, Ogola JBO, Mhizha T (2021) AquaCrop Model Calibration and Validation for Chickpea *(Cicer Arietinum)* in Southern Africa. Cogent Food Agric 7:1898135. 10.1080/23311932.2021.1898135
91. Toumi J, Er-Raki S, Ezzahar J, Khabba S, Jarlan L, Chehbouni A (2016) Performance Assessment of AquaCrop Model for Estimating Evapotranspiration, Soil Water Content and Grain Yield of Winter Wheat in Tensift Al Haouz (Morocco): Application to Irrigation Management. Agric Water Manage 163:219–235. 10.1016/j.agwat.2015.09.007
92. Minhas PS, Ramos TB, Ben-Gal A, Pereira LS (2020) Coping with Salinity in Irrigated Agriculture: Crop Evapotranspiration and Water Management Issues. Agric Water Manage 227:105832. 10.1016/j.agwat.2019.105832
93. Paz AM, Amezketa E, Canfora L, Castanheira N, Falsone G, Goncalves MC, Gould I, Hristov B, Mastrorilli M, Ramos T et al (2023) Salt-Affected Soils: Field-Scale Strategies for Prevention, Mitigation, and Adaptation to Salt Accumulation. Italian J Agron 18:2166. 10.4081/ija.2023.2166
94. Yu Q, Kang S, Hu S, Zhang L, Zhang X (2021) Modeling Soil Water-Salt Dynamics and Crop Response under Severely Saline Condition Using WAVES: Searching for a Target Irrigation Volume for Saline Water Irrigation. Agric Water Manage 256:107100. 10.1016/j.agwat.2021.107100
95. Sanad H, Moussadek R, Spaccini R, Paradiso R, Oueld Lhaj M, Zouahri A, Dakak H, Mouhir L (2026) Trace Metal Accumulation in Horticulture Production Systems (HPS) of Mediterranean Agro-Ecosystems: Origins, Impacts on Soil Health, Water Resources, and Plant Uptake with Sustainable Mitigation Strategies. Front Sustain Food Syst 10:1803164. 10.3389/fsufs.2026.1803164
96. Rhoades JD, Kandiah A, Mashali AM, Rhoades JD (1992) *The Use of Saline Waters for Crop Production*; FAO irrigation and drainage paper; Food and Agriculture Organization of the United Nations: Rome, ; ISBN 978-92-5-103237-4
97. Li Y, Feng Q, Li D, Li M, Ning H, Han Q, Hamani AKM, Gao Y, Sun J (2022) Water-Salt Thresholds of Cotton (Gossypium Hirsutum L.) under Film Drip Irrigation in Arid Saline-Alkali Area. Agriculture 12:1769. 10.3390/agriculture12111769
98. Dirk RAES, Pasquale STEDUTO, Theodore C, Hsiao E, Fereres (eds) (2012) ; FAO irrigation and drainage paper; Food and Agriculture Organization of the United Nations: Rome, ; ISBN 978-92-5-107274-5

Figures

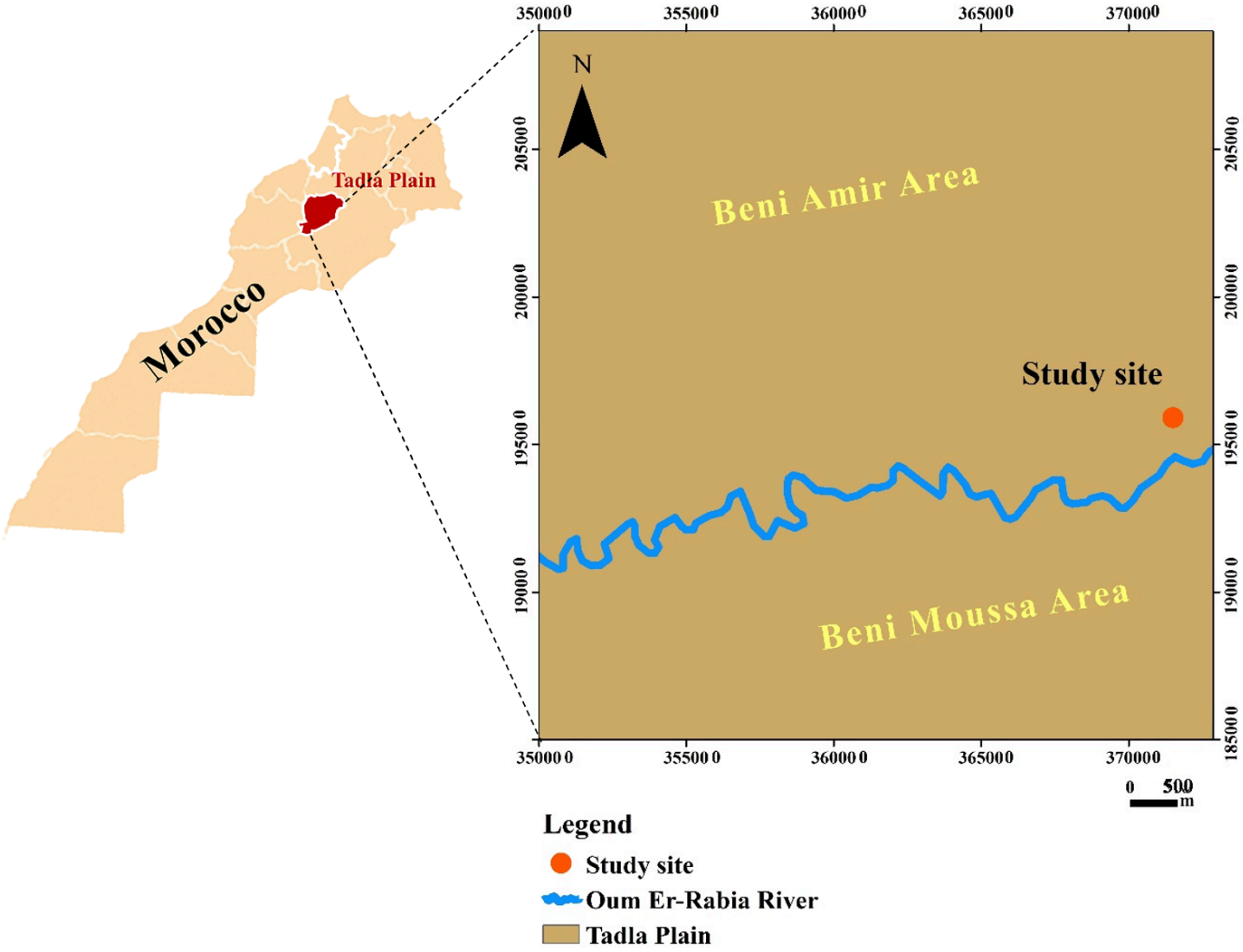


Figure 1

Location of the study area in the Tadla plain, central Morocco.

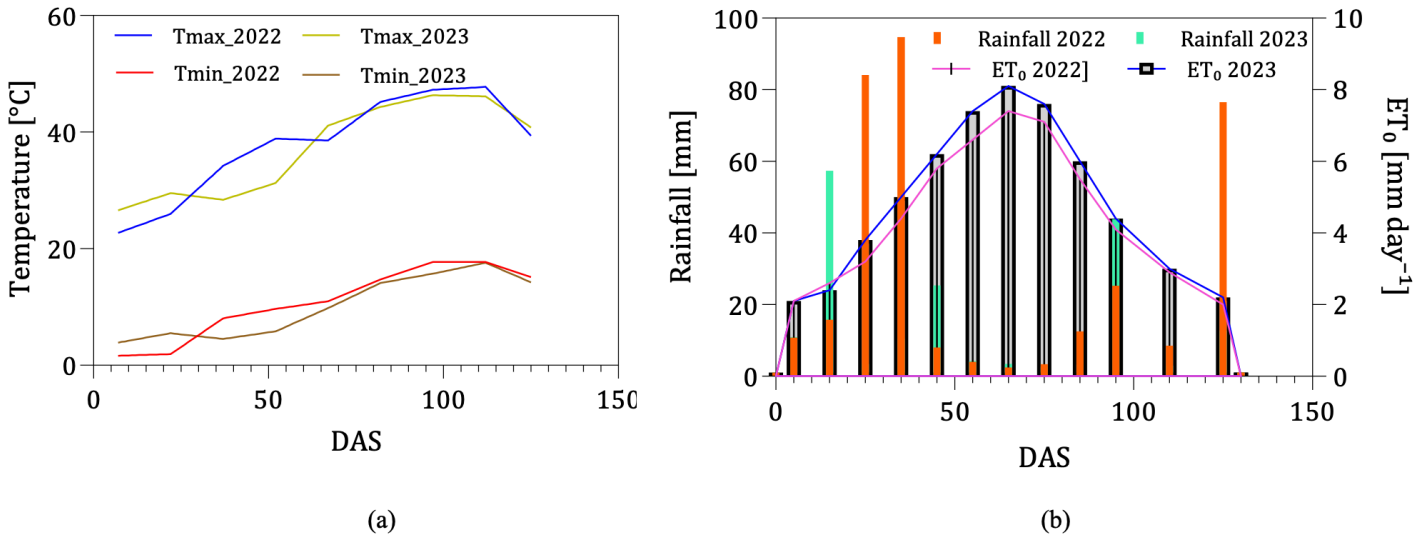


Figure 2

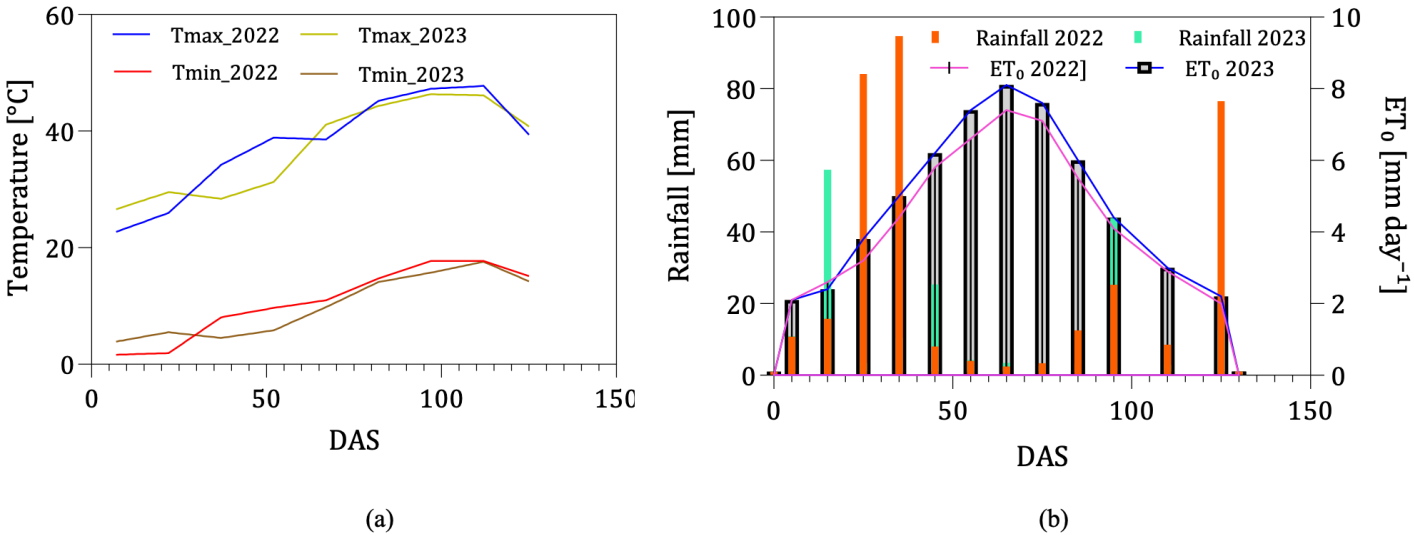


Figure 2

Seasonal variations in (a) daily maximum and minimum air temperatures (Tmax and Tmin) and (b) reference evapotranspiration (ET_0) and monthly precipitation during the 2022 and 2023 growing seasons.

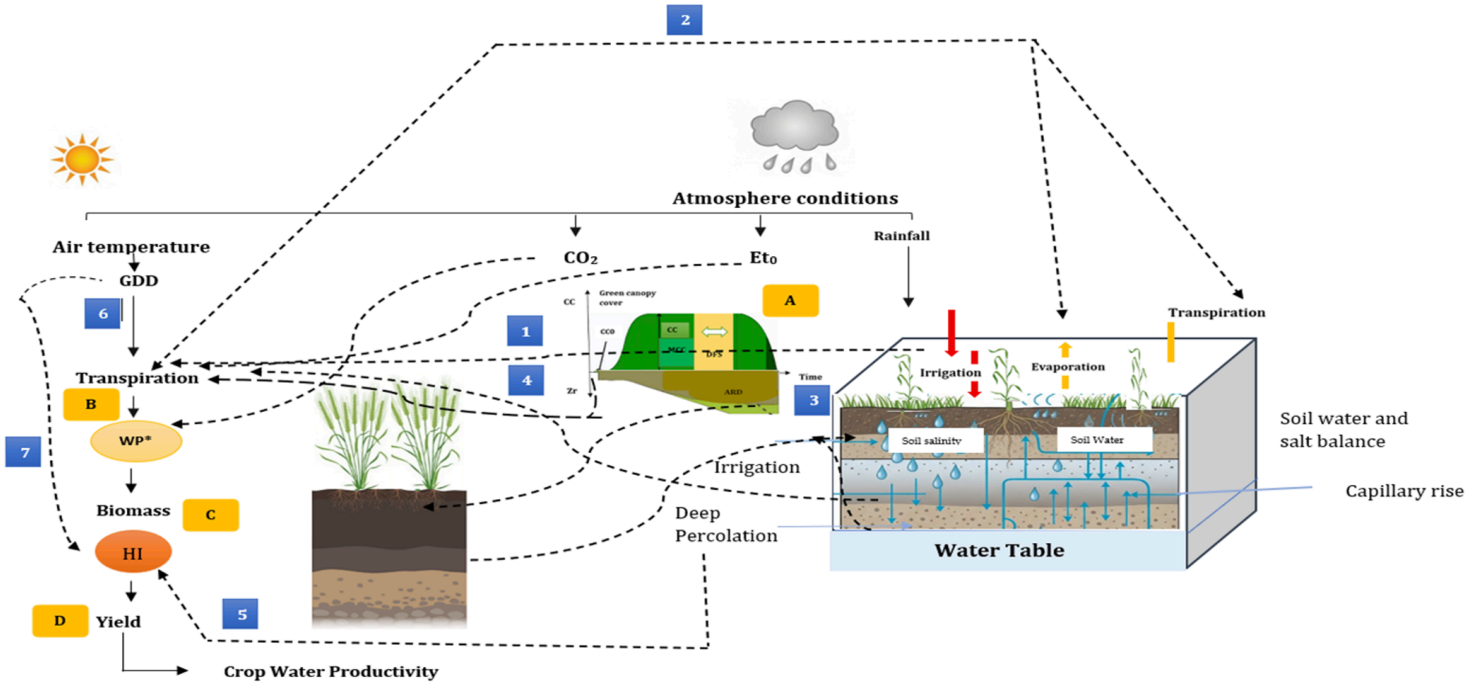


Figure 3

Calculation scheme of the AquaCrop model, showing the four sequential steps (A–D) and the associated processes (dotted arrows) affected by water stress (1–5) and temperature stress (6–7). CC is the green canopy cover; Zr is the rooting depth; CGC is the canopy growth coefficient; CDC is the canopy decline coefficient; GDD is the growing degree days; ET0 is the reference evapotranspiration; WP is the normalized biomass water productivity; and HI is the harvest index. Water stress: (1) slows canopy expansion, (2) accelerates canopy senescence, (3) decreases root deepening

(only under severe stress), (4) reduces stomatal conductance and transpiration, and (5) affects the harvest index. Cold temperature stress (6) reduces crop transpiration, while extreme temperature stress (7) inhibits pollination and reduces HI [60].

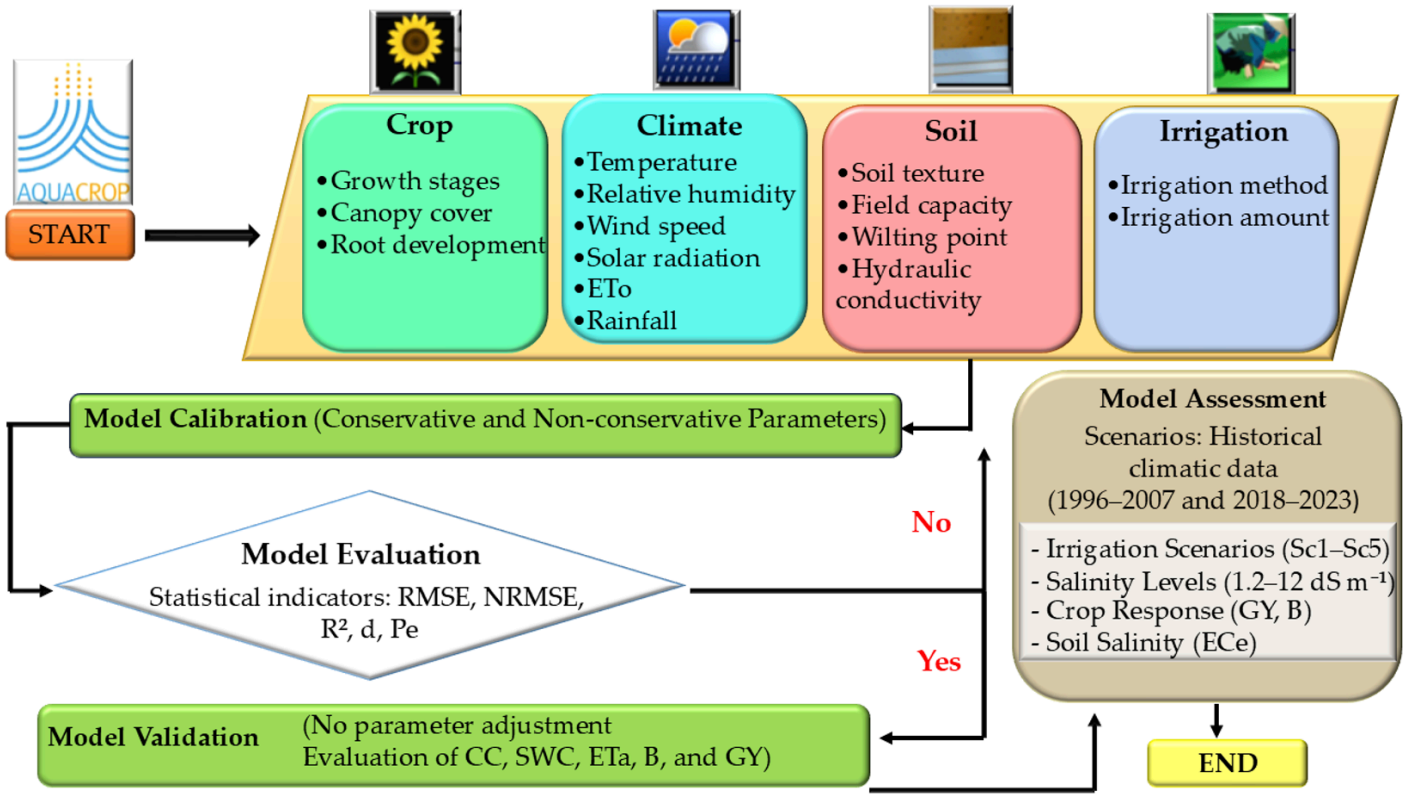


Figure 4

Flowchart of the AquaCrop model for simulating winter wheat.

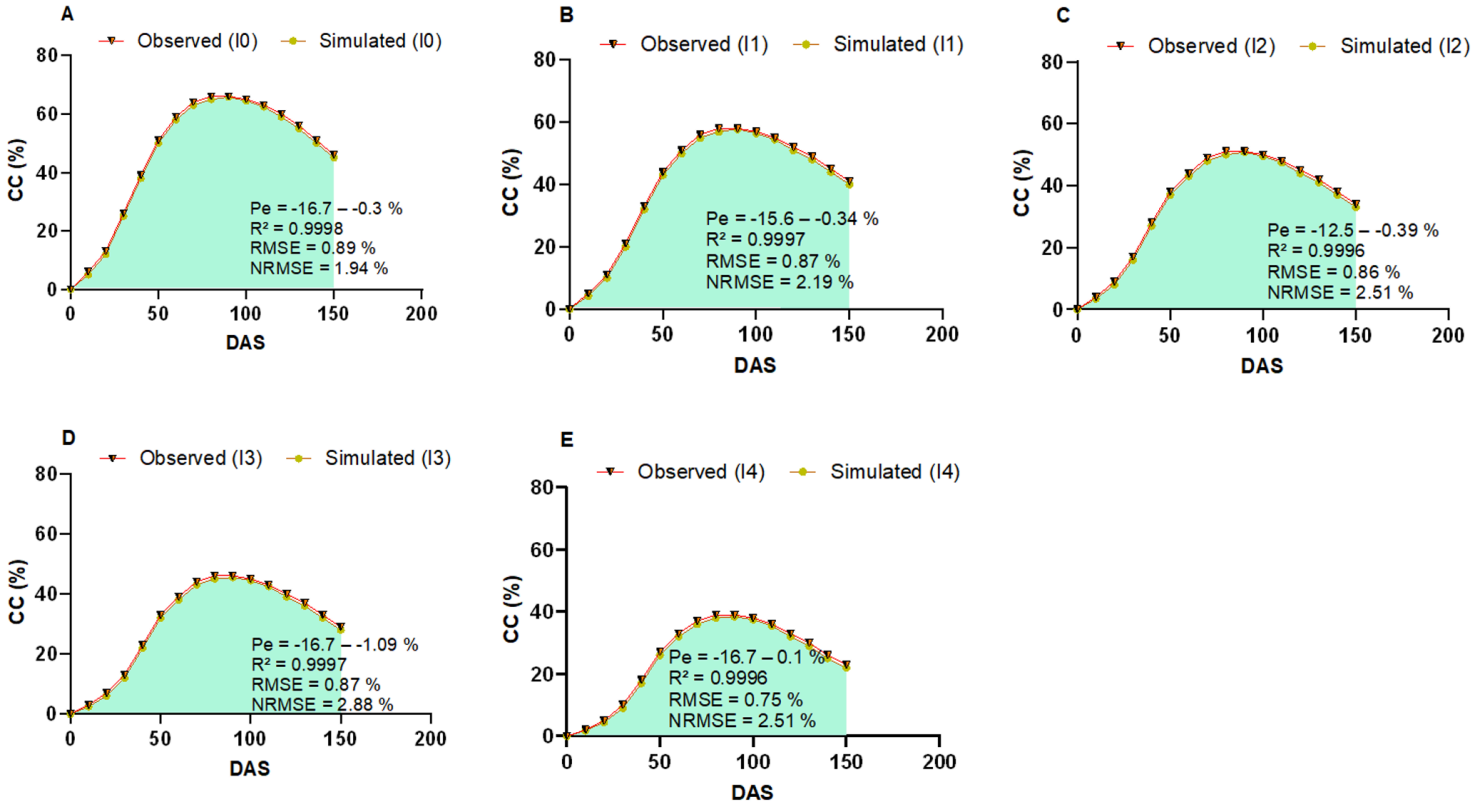


Figure 5

Calibration of canopy cover (CC) for winter wheat during the 2023 growing season under different salinity treatments (I0–I4).

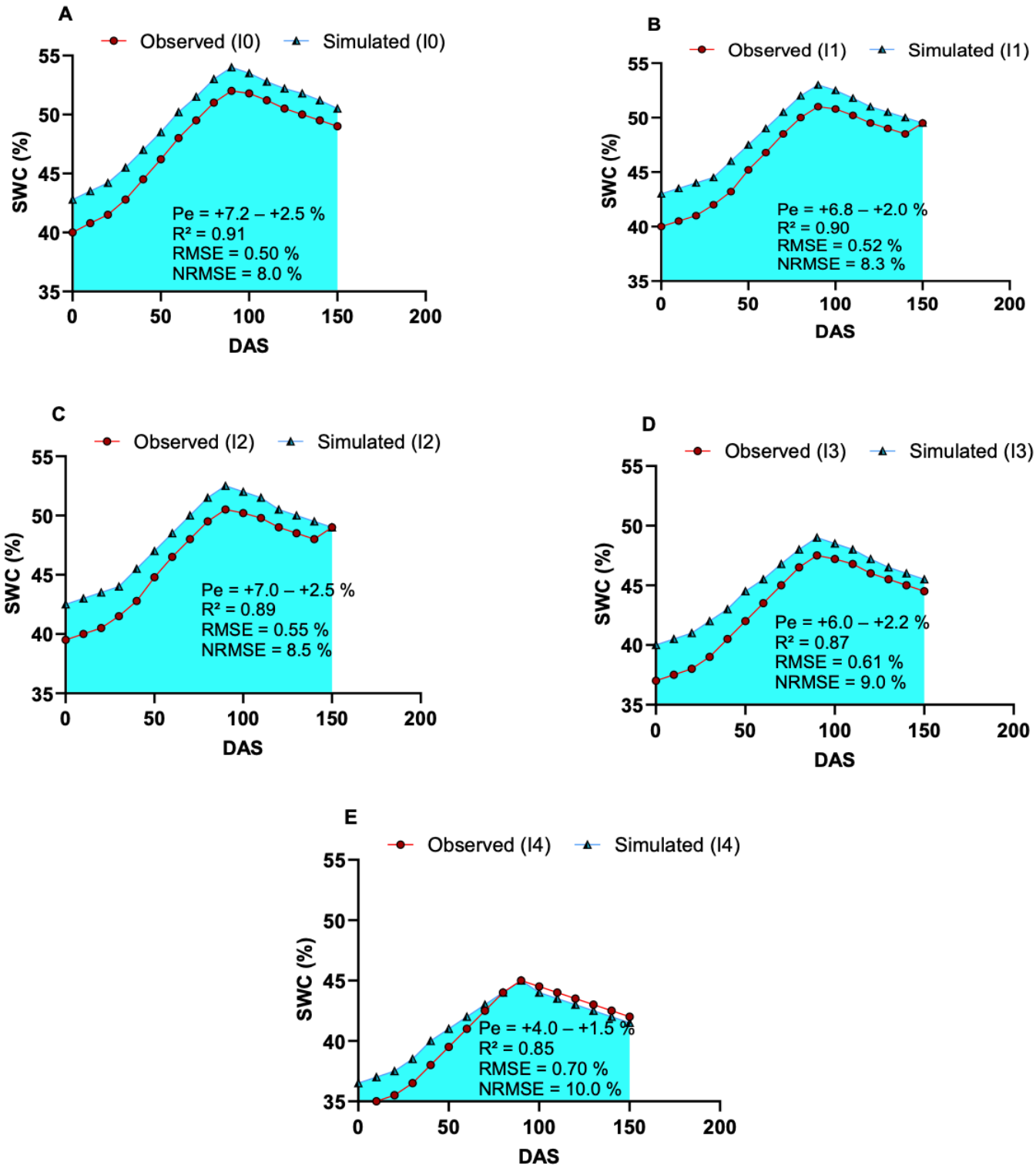


Figure 6

Calibration of soil water content (SWC) for winter wheat during the 2023 growing season under different salinity treatments (I_0–I_4). Sub-panels represent each irrigation–salinity treatment: A = I0, B = I1, C = I2, D = I3, E = I4. Observed and simulated SWC values are plotted over Days After Sowing (DAS). The blue shaded area represents the deviation between simulated and observed soil water content over time.

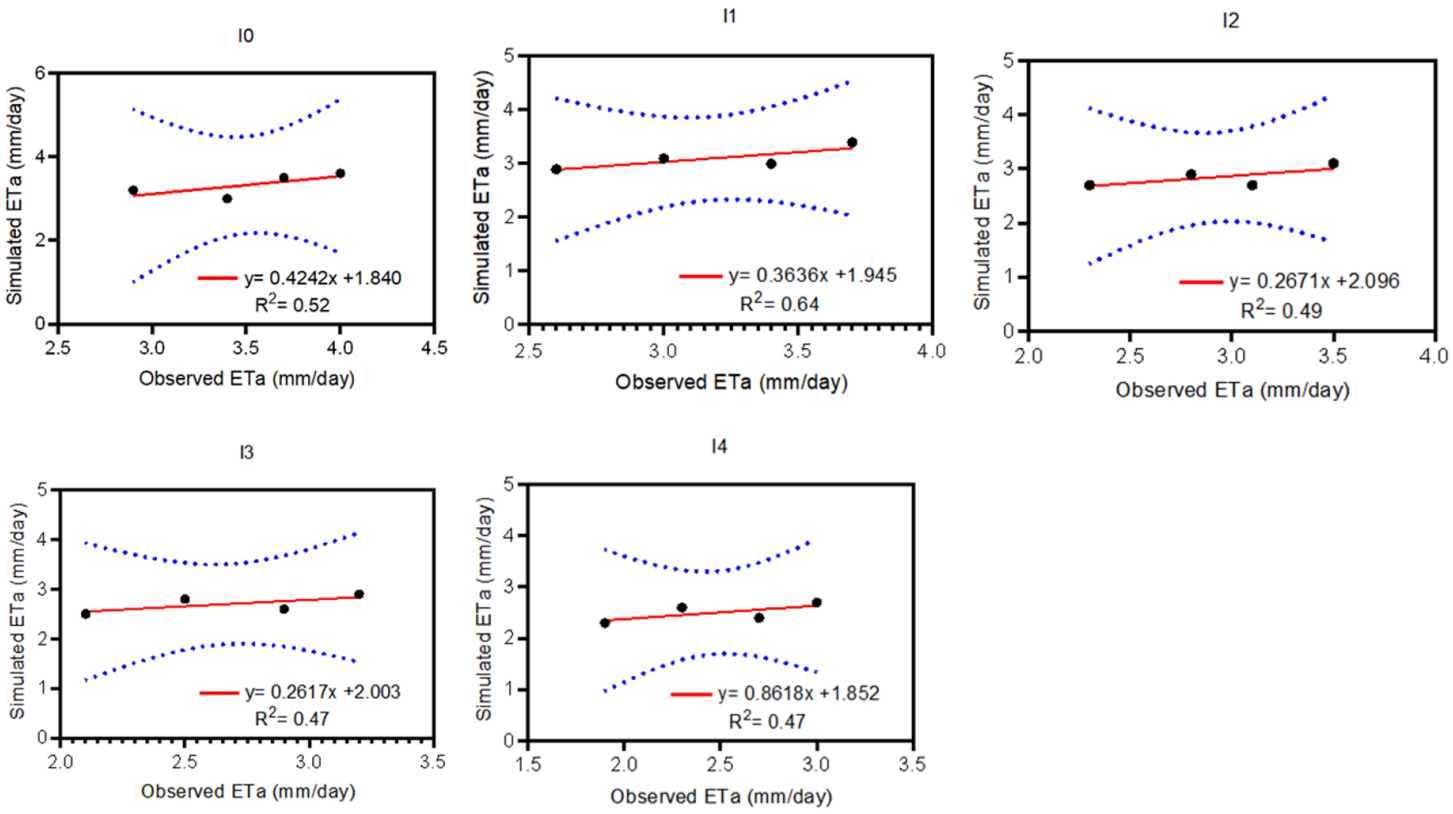


Figure 7

Simulation of actual evapotranspiration (ETa) for winter wheat during the 2023 growing season under irrigation treatments (I0–I4). Panels (**a–e**) correspond to I0, I1, I2, I3, and I4. Observed ETa is plotted on the x-axis and simulated ETa on the y-axis. The solid line represents the linear regression between observed and simulated values, with the corresponding equation and R^2 indicated in each panel. The dotted curves represent the dispersion around the regression line.

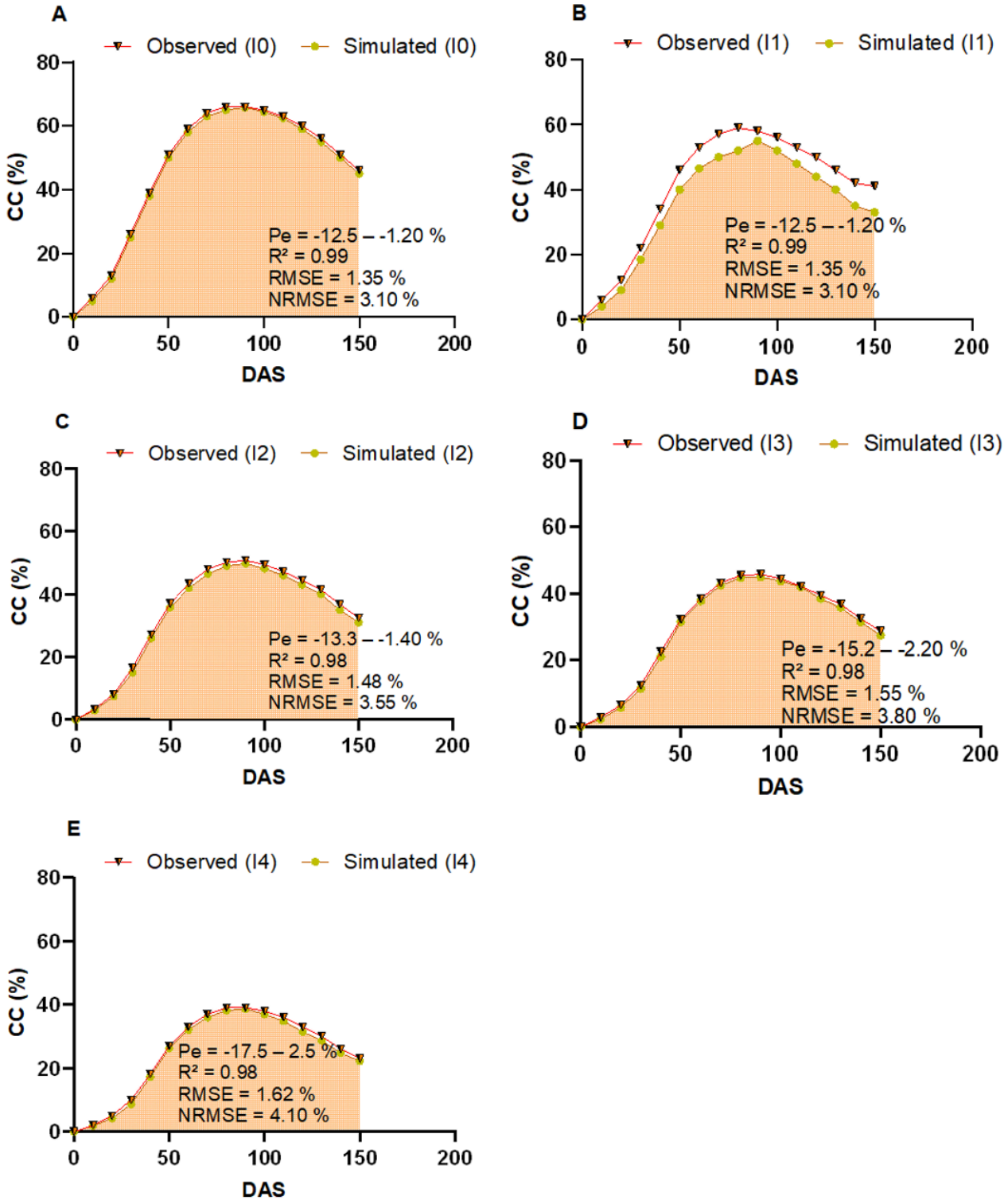


Figure 8

Validation of canopy cover (CC) for winter wheat during the 2022 growing season under salinity treatments (I0–I4). Panels (a–e) correspond to I0, I1, I2, I3, and I4, respectively. Observed and simulated CC are plotted against days after sowing (DAS). The shaded area represents the de-viation between simulated and observed values.

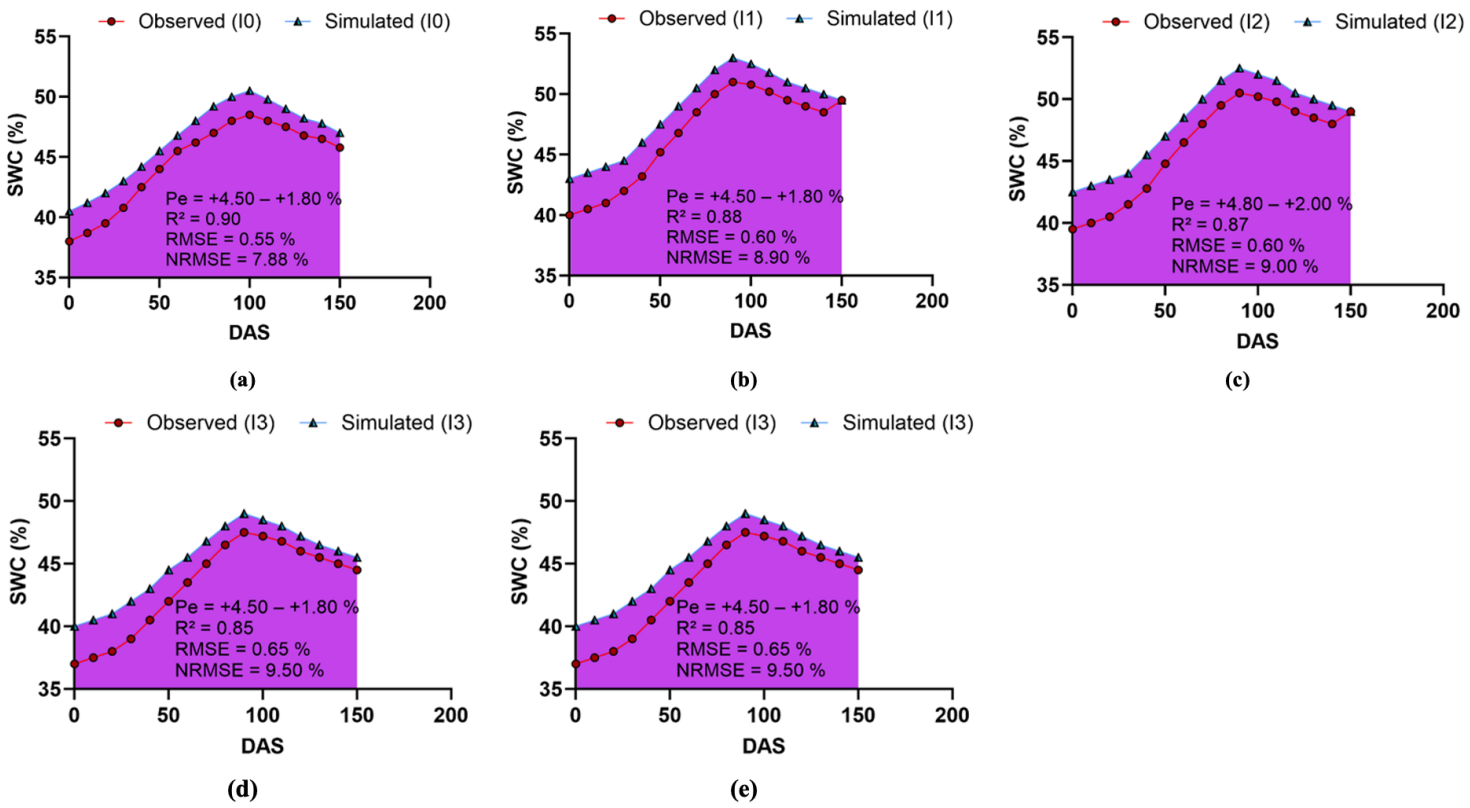


Figure 9

Validation of soil water content (SWC) for winter wheat during the 2022 growing season under salinity treatments (I0–I4).

Observed (I0)
Simulated (I0)
SWC (%)
DAS
Pe = +4.50 – +1.80 %
R² = 0.90
RMSE = 0.55 %
NRMSE = 7.88 %
(a)
Observed (I1)
Simulated (I1)
Pe = +4.50 – +1.80 %
R² = 0.88
RMSE = 0.60 %
NRMSE = 8.90 %
(b)
Observed (I2)
Simulated (I2)
Pe = +4.80 – +2.00 %
R² = 0.87
RMSE = 0.60 %
NRMSE = 9.00 %
(c)
Observed (I3)
Simulated (I3)
Pe = +4.50 – +1.80 %
R² = 0.85
RMSE = 0.65 %
NRMSE = 9.50 %
(d)
Observed (I3)
Simulated (I3)
Pe = +4.50 – +1.80 %
R² = 0.85
RMSE = 0.65 %
NRMSE = 9.50 %
(e)

Figure 9

Validation of soil water content (SWC) for winter wheat during the 2022 growing season under salinity treatments (I0–I4).

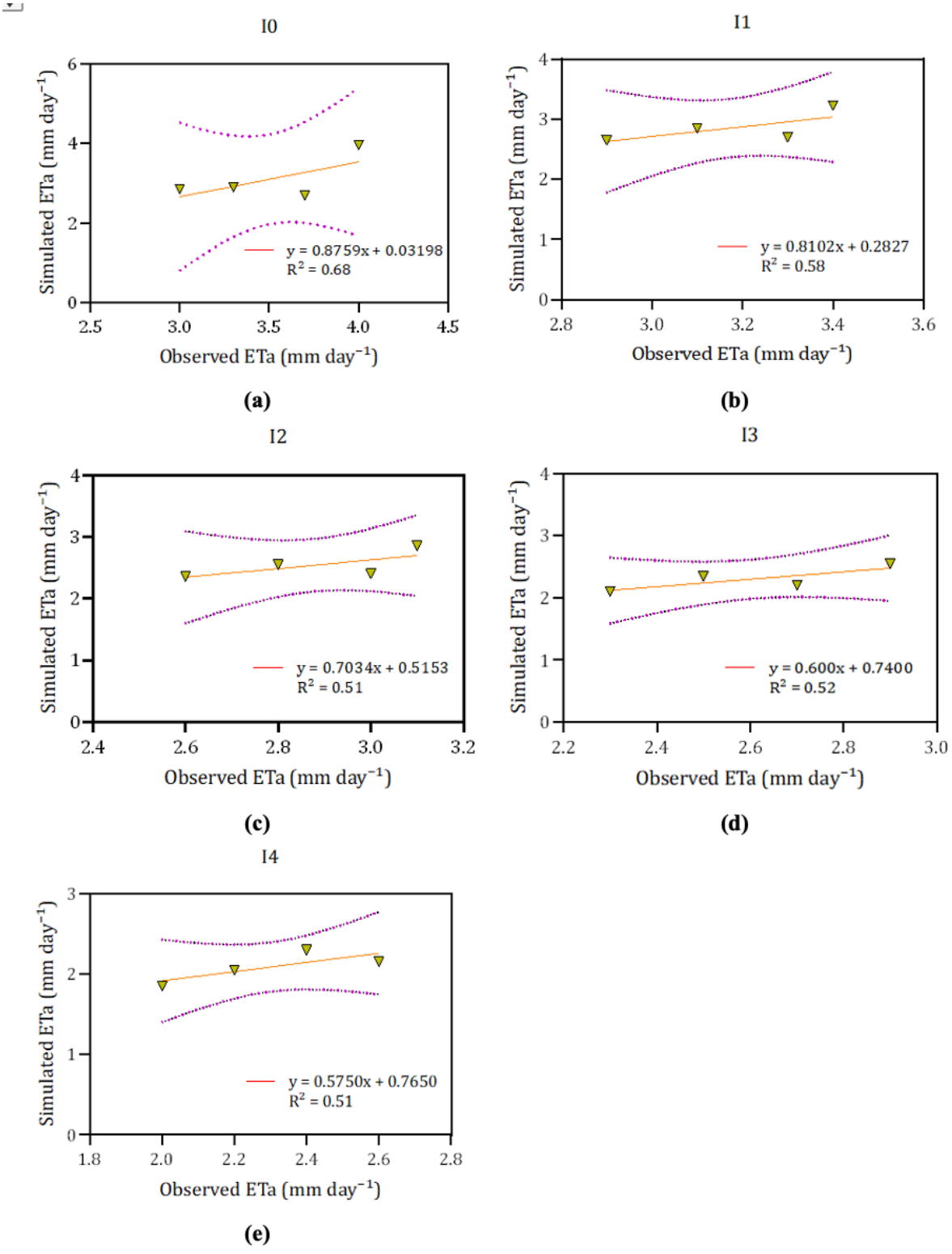


Figure 10

Validation of actual evapotranspiration (ETa) for winter wheat during the 2022 growing season under irrigation treatments (I0–I4).

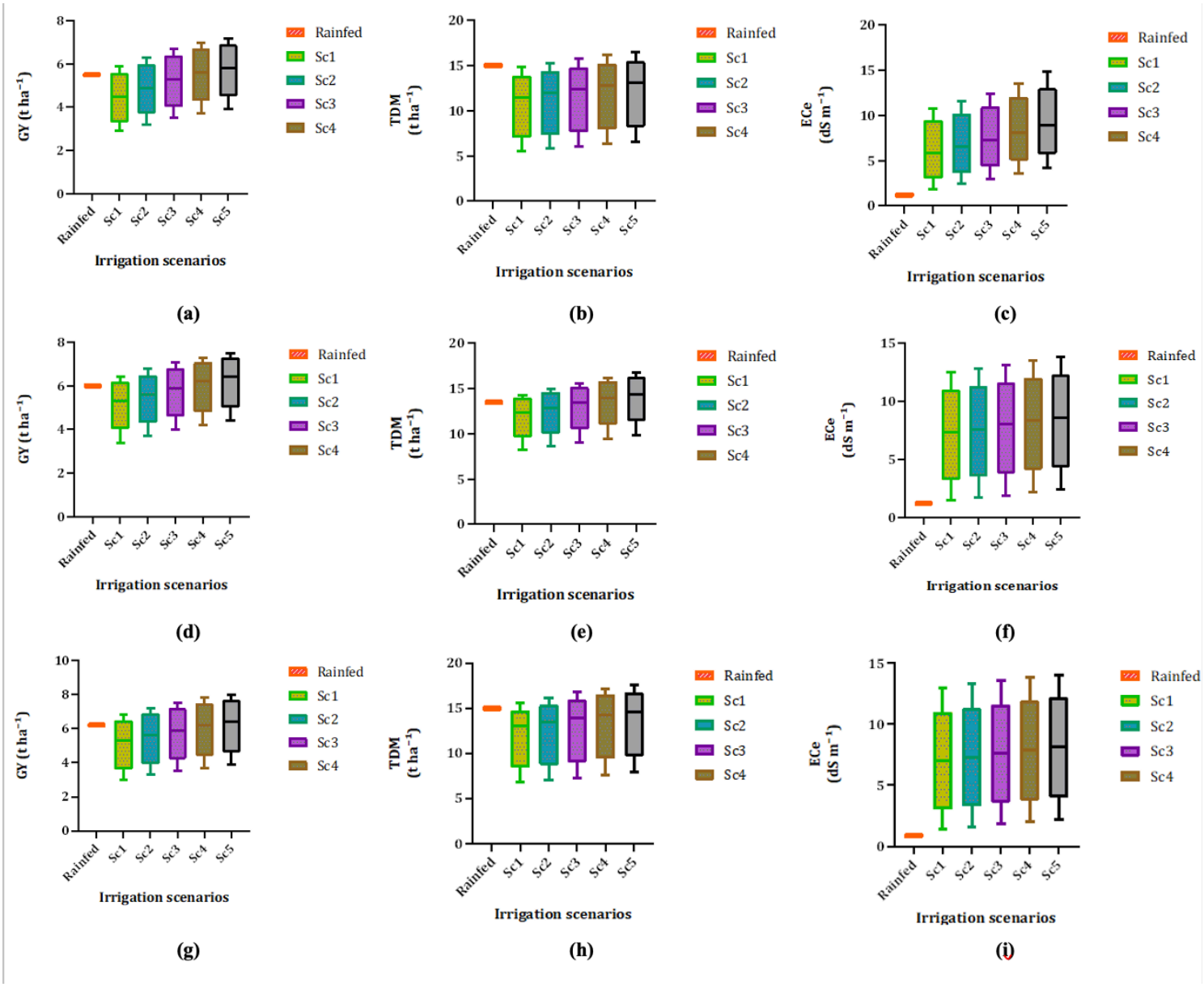


Figure 11

Estimated grain yield (GY), biomass (B), and soil electrical conductivity (ECe) under different saline irrigation scenarios (1996–2007 and 2018–2023). Panels (**A–C**), (**D–F**), and (**G–I**) represent dry, normal, and wet years, respectively.

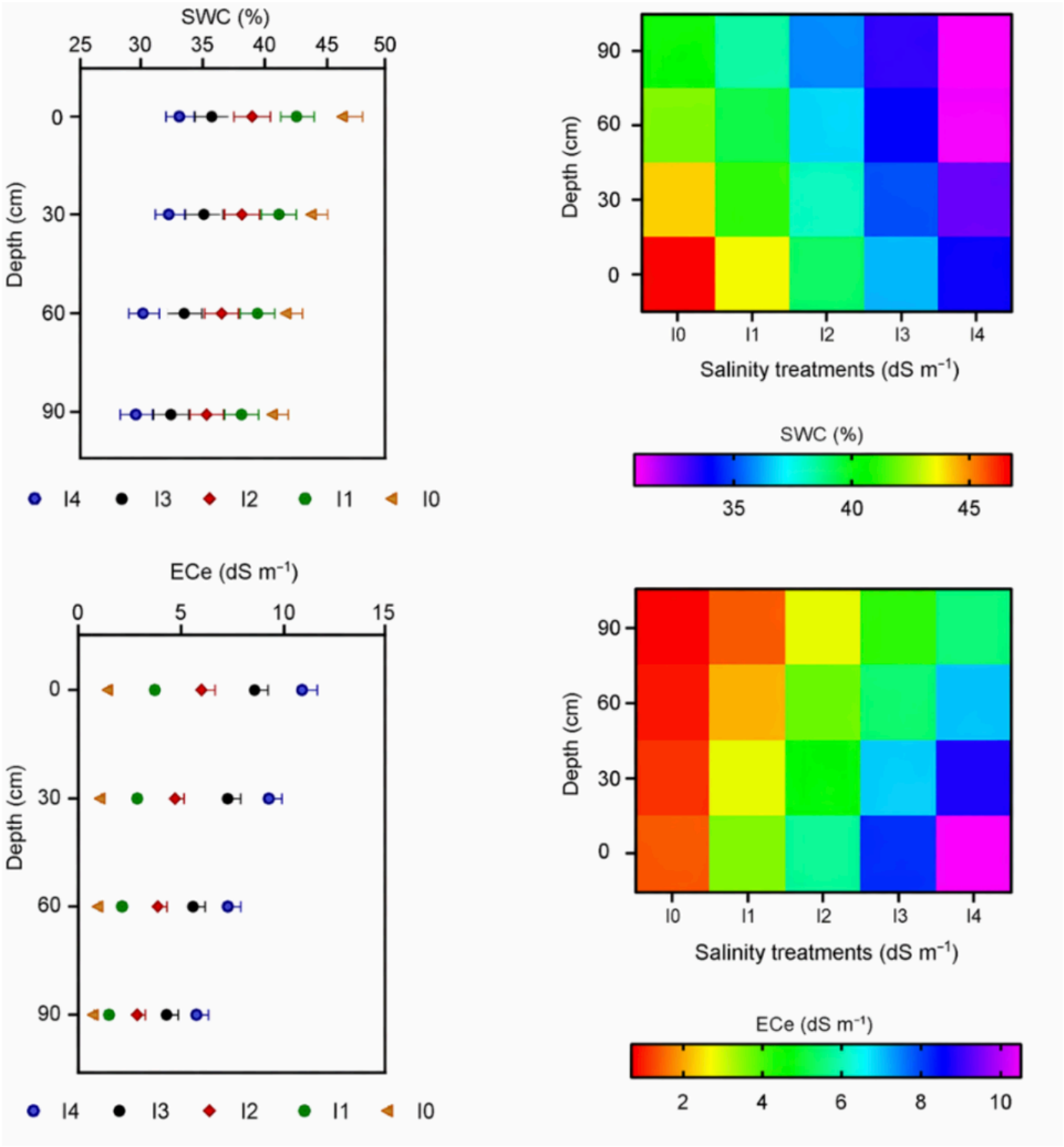

SWC (%)
25
30
35
40
45
50
0
30
60
90
Depth (cm)
I4
I3
I2
I1
I0
Depth (cm)
90
60
30
0
I0
I1
I2
I3
I4
Salinity treatments (dS m-1)
SWC (%)
35
40
45
ECe (dS m-1)
0
5
10
15
0
30
60
90
Depth (cm)
I4
I3
I2
I1
I0
Depth (cm)
90
60
30
0
I0
I1
I2
I3
I4
Salinity treatments (dS m-1)
ECe (dS m-1)
2
4
6
8
10

Figure 12

13

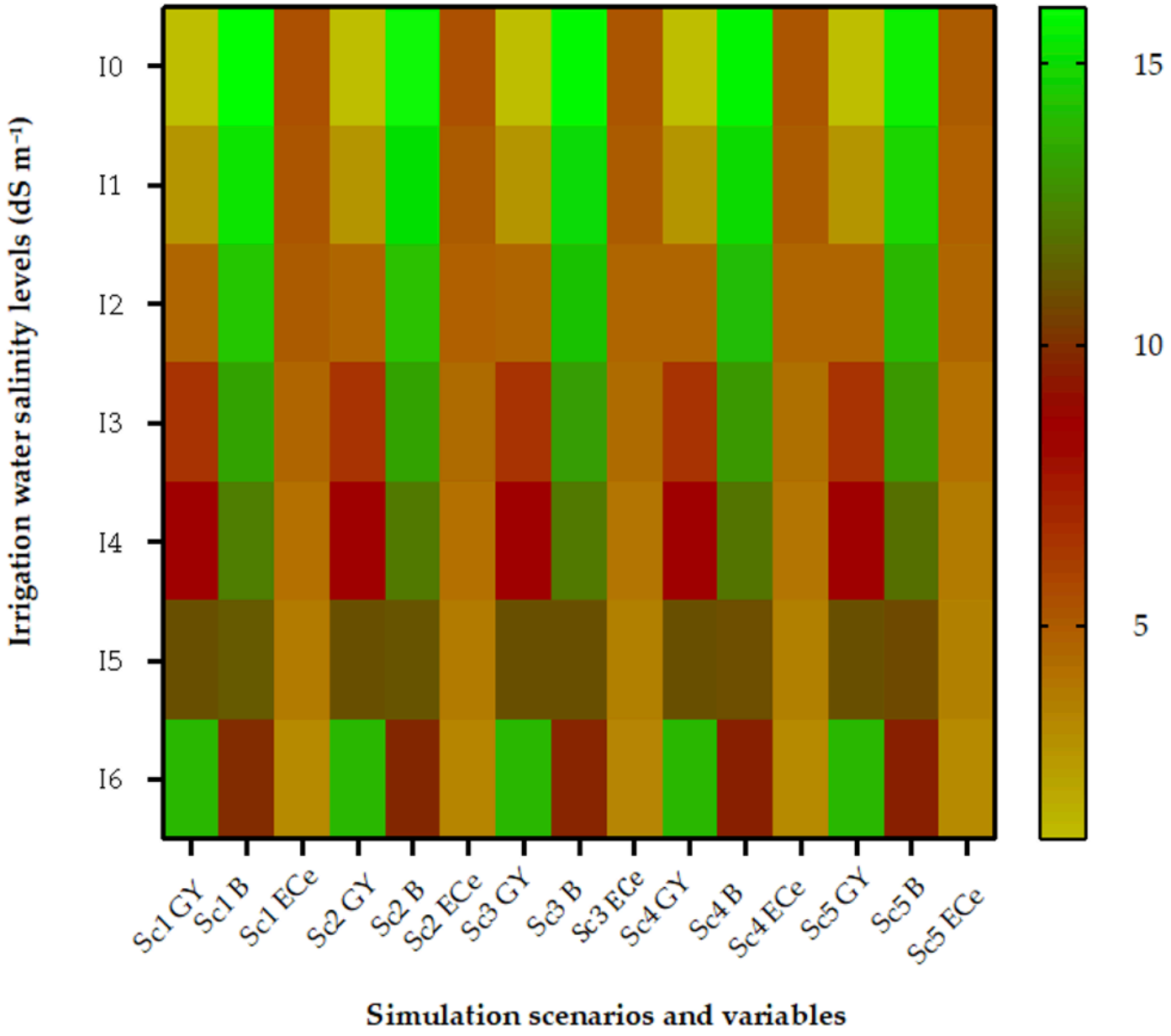


Figure 12

Heatmap illustrating relationships between grain yield (GY), above-ground biomass (B), and soil electrical conductivity (ECe) across irrigation-water salinity levels (I0–I6) and simulation scenarios (Sc1–Sc5).

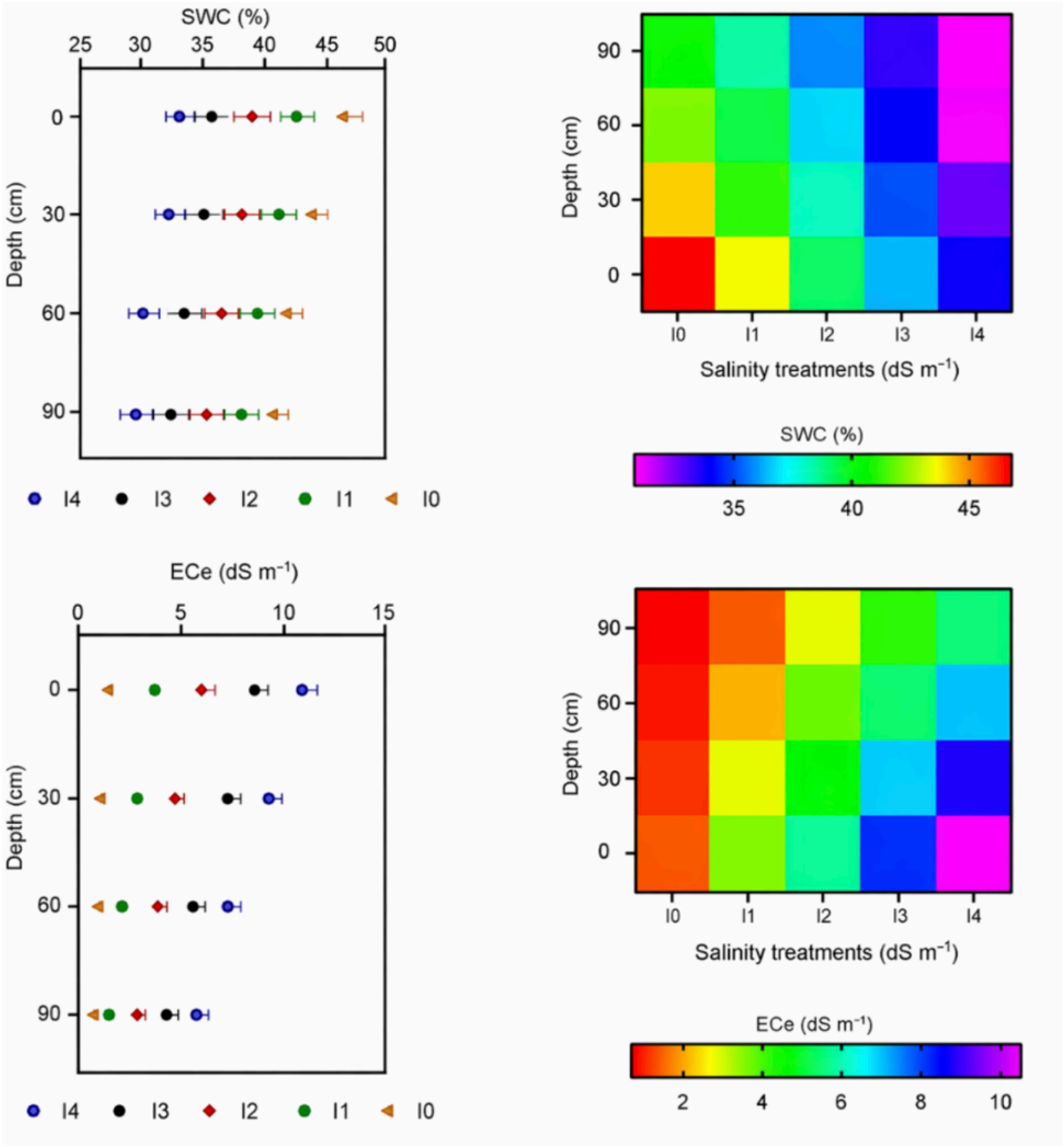


Figure 13

Vertical distribution of soil water content (SWC) and soil electrical conductivity (ECe) under saline irrigation treatments (I0–I4).